ADVANCED ENERGY MATERIALS
www.advenergymat.de

Revealing the Potential and Challenges of High-Entropy Layered Cathodes for Sodium-Based Energy Storage

Hong Gao, Jiayi Li, Fan Zhang, Congcong Li, Jun Xiao, Xinming Nie, Guilai Zhang, Yang Xiao, Dingyi Zhang, Xin Guo,* Yong Wang, Yong-Mook Kang, Guoxiu Wang,* and Hao Liu**

Sodium-ion batteries (SIBs) reflect a strategic move for scalable and sustainable energy storage. The focus on high-entropy (HE) cathode materials, particularly layered oxides, has ignited scientific interest due to the unique characteristics and effects to tackle their shortcomings, such as inferior structural stability, sluggish reaction kinetics, severe Jahn-Teller effects induced lattice distortion, and poor oxygen reversibility at high voltage. This review focuses on high-entropy oxide materials, highlighting their fundamentals, design principles, and application in layered oxide cathodes for SIBs. It delves into the growth mechanism, composition-properties correlations, and the functional roles of high-entropy design in enhancing the performance of layered oxide cathodes. Furthermore, it furnishes a comprehensive survey of recent advancements and persisting challenges within the domain of layered high-entropy cathode materials, as well as offers insights into potential future research directions in line with the current state of knowledge.

1. Introduction

Sodium-ion batteries (SIBs) are emerging as a cost-effective alternative to lithium-ion batteries (LIBs) due to the abundant availability of sodium.[1–4] The growing utilization of intermittent clean energy sources and efficient grid electricity has spurred research on sustainable SIBs, providing scalable and environmentally conscious energy storage solutions.[5–8] However, the larger radius of Na^+ and inherent limitations of electrode materials, particularly for typical cathodes such as sodium layer oxides and Prussian blue analogues, hamper the performance of SIBs.[9–11] Recently, the high-entropy strategy stands out among other modification methods due to its unique composition and structure. By introducing a diverse array of elements, the configurational entropy within the lattice is increased, resulting in a decreased Gibbs free energy, varied crystal structures and heightened structural stability. Concurrently, certain selectively incorporated elements serve a role analogous to doping strategies. Therefore, this approach amalgamates the merits of entropy configuration and doping effects, efficiently suppressing detrimental phase transitions. This leads to enhanced the structural stability and ionic conductivity in materials, thereby contributing to prolonged cycle life and improved charge/discharge rates.

H. Gao, J. Li, F. Zhang, C. Li, G. Zhang, Y. Xiao, D. Zhang, Y. Wang
Joint International Laboratory on Environmental and Energy Frontier Materials
School of Environmental and Chemical Engineering
Shanghai University
Shanghai 200444, China

J. Xiao, X. Guo
Faculty of Materials Science and Energy Engineering
Institute of Technology for Carbon Neutrality
Shenzhen Institute of Advanced Technology
Chinese Academy of Sciences
Shenzhen, Guangdong 518055, China
E-mail: x.guo1@siat.ac.cn

The ORCID identification number(s) for the author(s) of this article can be found under https://doi.org/10.1002/aenm.202304529

DOI: 10.1002/aenm.202304529

X. Nie
School of Physics and Electronic Engineering
Jiangsu Normal University
Xuzhou, Jiangsu 221116, China
E-mail: nxinming@jsnu.edu.cn

Y.-M. Kang
Department of Materials Science & Engineering
Korea University
Seoul 02841, Republic of Korea

G. Wang, H. Liu
Centre for Clean Energy Technology
University of Technology Sydney
Broadway, Sydney, NSW 2007, Australia
E-mail: Guoxiu.Wang@uts.edu.au; hao.liu@uts.edu.au

High-entropy oxides (HEOs) are an emerging and intriguing class of oxides distinguished by their distinctive composition, often amalgamating equal or substantial proportions of five or more elements, resulting in materials with heightened configurational entropy.[12,13] In 2015, Rost and colleagues introduced the pioneering concept of "high entropy oxides" (HEOs).[24] They compellingly demonstrated the role of entropy in orchestrating the reversible transition from multi-phase to single-phase configurations within materials, influencing the thermodynamic processes. This deliberate combination of diverse primary elements results in materials with heightened configurational entropy, bestowing upon them a range of exceptional characteristics, such as outstanding ionic conductivity and strong structural stability.[14–23] Significant advancements have been achieved in developing cathode materials based on HEOs, each exhibiting distinct electrochemical performance characteristics. Ceder and his team took the lead in exploring high entropy disordered rock salt (DRX) cathode materials by incorporating multiple transition metal species into the structure. This approach increased metal redox capacity and addressed challenges in short-range ordering, enhancing lithium transport in cation-disordered rocksalt cathodes. The DRX cathode with six TM species maintained a capacity of 170 mAh g^{-1} at a high rate of 2000 mA g^{-1}.[26] Moreover, Ceder and his team demonstrated the introduced distortions in high-entropy materials lead to a convergence of site energies for alkali ions, facilitating percolation with low activation energy. Experimental verification highlights the substantial enhancement of ionic conductivities across diverse structures due to high entropy.[27] Considering cost, Xin et al. achieved a zero-strain, zero-cobalt and high-nickel layered $LiNi_{0.8}Mn_{0.13}Ti_{0.02}Mg_{0.02}Nb_{0.01}Mo_{0.02}O_2$ cathode (HE-LNMO) through compositionally complex high-entropy doping. HE-LNMO exhibited exceptional stability and capacity retention, paving the way for the practical application of Co-free cathodes.[28] A pioneering high-entropy layered oxide cathode $NaNi_{0.12}Cu_{0.12}Mg_{0.12}Fe_{0.15}Co_{0.15}Mn_{0.1}Ti_{0.1}$-$Sn_{0.1}Sb_{0.04}O_2$ for SIBs realized reversible O3-P3 phase transition and cationic redox, exhibits enhanced cycling stability, retaining ≈ 83% of its initial capacity after 500 cycles.[25] These findings introduced a guiding principle with profound implications for the design and development of high-entropy cathodes.

Layered oxide cathodes are favored among other candidates owing to the high energy density, ease of fabrication, and presence of 2D ion migration channels between layers.[23,29,30] The development of high-entropy layered oxides, achieved by incorporating appropriate elements into the structure, has been demonstrated as an effective solution for tackling challenges such as inferior structural stability derived from phase transitions, Jahn-Teller effect-induced lattice distortion, and poor reversibility of oxygen redox. This is due to the improved stability of high-entropy layered oxides when compared to conventional materials.[31] This review provides a comprehensive overview of recent research progress, future prospects, and the challenges faced in the development of layered high-entropy cathodes for SIBs. We also emphasize the design principle of HEOs, delving into their formation mechanism and clarifying the composition-properties correlations, aiming to unravel the intricate details of influential elements and the evolution of crystal and electronic structures during sodium (de)intercalation. Meanwhile, the functional roles of high-entropy structures in achieving excellent performance and their typical applications have been classified and discussed insightfully.

2. Fundamentals of High Entropy Oxide (HEO) Materials

The extensive range for compositional adjustments and the diverse crystal structures make HEOs promising for various applications, such as protective coatings,[46,47] energy storage,[48,49] and catalysis.[50,51] In the energy storage field, the HEOs with a combination of active and inactive transition metal (TM) elements would lead to a minor reduction in capacity, primarily attributed to the decrease in redox couples. Achieving a balance between high entropy and high capacity can be attained through fine-tuning the concentration of individual TMs.[52] Indeed, delving deeper into the fundamental mechanisms governing the interplay between high-entropy configurations and their impact on the structure-property relationship. In this section, by introducing high-entropy materials, design principles and crystal evolution of HEO formation, we aim to enhance our understanding of the intricate relationships between composition and properties in HEO materials, and offer insights into the underlying mechanisms that shape their behavior and characteristics.

2.1. Defining High Entropy Materials

The process of entropy stabilization involves enhancing configurational entropy (S_{config}), ultimately resulting in the stabilization of a single-phase crystal structure. This is achieved by introducing more elements randomly distributed across the same lattice positions. The molar configurational entropy of oxide systems can be computed using equation (1):[32,33]

$$\Delta S_{config} = -R\left[\left(\sum_{i=1}^{N} x_i \ln x_i\right)_{cation-site} + \left(\sum_{j=1}^{N} x_j \ln x_j\right)_{anion-site}\right] \quad (1)$$

Where R denote the universal gas molar constant (R = 8.314). x_i and x_j is the molar fractions of anions and cations, respectively, and N represents the number of elemental species. Expanding the number of elements in a system leads to an increase in S_{config}. For instance, consider a P2-type 3-cation oxide $Na_{2/3}Ni_{1/3}Mn_{1/3}Fe_{1/3}O_2$ with an entropy value of 1.10. However, when transitioning to a 4-cation oxide $Na_{2/3}Ni_{1/3}Mn_{1/3}Fe_{1/3-x}Al_xO_2$, the entropy value increases to 1.28R.[81] When each element's molar ratio is equal, the system's configurational entropy reaches its maximum.[34] In a system with five cations at equiatomic proportions, the highest achievable S_{config} value is 1.61 R. Based on configurational entropy classification,[32] materials with $S_{config} < 1$ R are considered "low entropy", those with 1.5 R > $S_{config} \geq 1$ R are "medium entropy", while materials with $S_{config} \geq 1.5$ R are categorized as "high entropy" systems. Thereby, the high-entropy systems intentionally incorporate a substantial proportion of multiple elements in roughly equal amounts, creating materials with significant configurational entropy. This approach goes beyond trace doping, distinguishing itself from conventional doping practices and is

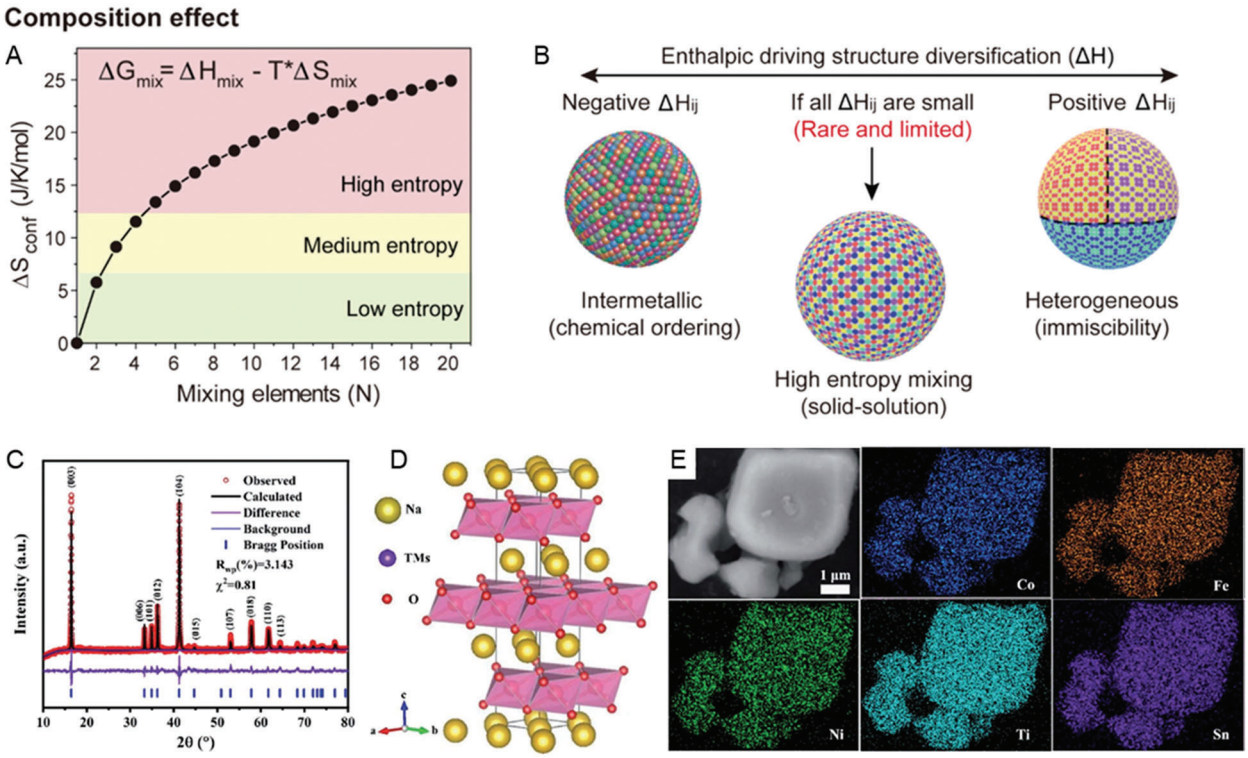

Figure 1. Thermodynamic analysis of high-entropy mixing considers both entropy A) and enthalpy B), which are mainly determined by the composition of HE materials. Reproduced with permission.[41] Copyright 2022, American Association for the Advancement of Science. C) XRD and Rietveld pattern, D) structure schematic and E) SEM-EDS mapping of the O3-NFCNTSL cathode. Reproduced with permission.[55] Copyright 2022, Royal Society of Chemistry.

characterized by a more balanced and extensive compositional diversity.

The impact of entropy on phase stability of compounds can be comprehended by examining the Gibbs free energy of mixing (ΔG_{mix}):[35–40]

$$\Delta G_{mix} = \Delta H_{mix} - T\Delta S_{mix} \quad (2)$$

In equation (2), ΔH_{mix} represents the mixing enthalpy, ΔS_{mix} is the mixing entropy, and ΔS_{config} typically dominates ΔS_{mix}. T denotes the absolute temperature. In numerous instances, a single phase can be attained when $S_{config} \geq 1.5$ R. In such cases, the dominance of $T\Delta S_{mix}$ term in the free energy landscape, overcoming ΔH_{mix}, resulting in a negative overall ΔG_{mix}, establishing entropy stabilization (**Figure** 1A,B).[41] It's important to note that entropy is directly tied to temperature, and elevated-temperature synthesis tends to promote the formation of a single-phased system with increased configurational entropy.[42–45]

2.2. Design Principle of HEO Cathodes

Typically, the design of a HEO cathode hinges on two pivotal factors: i) the promotion of disorder among TMs. This goal can be accomplished through a meticulous selection of elements, ensuring that their ionic radii differences fall within a range of 15%. For instance, it is impossible to synthesize sodium superionic conductors (NASICONs) materials containing five equimolar M^{4+} metal cations (Ge, Ti, Zr, Sn, Hf), likely due to the substantial size difference between Ge^{4+} and the other metal cations;[27] ii) the selected elements must provide charge compensation, thereby significantly improving electrochemical performance.[53,54]

Based on these criteria, Wang et al. prepared a six-component layered HEO O3–Na($Fe_{0.2}$ $Co_{0.2}Ni_{0.2}Ti_{0.2}Sn_{0.1}Li_{0.1}$)$O_2$ (O3-NFCNTSL) as a cathode material for SIBs.[55] The selected elements (Fe^{3+}, Ni^{2+}, Co^{3+}, Ti^{4+}, Sn^{4+}) have ionic radii smaller than 15%, facilitating the creation of disorder among TMs (Figure 1C–E). Meanwhile, the Fe^{3+}, Ni^{2+} and Co^{3+} can offer charge compensation and enhance the electrochemical performance, evidenced by the ex situ X-ray absorption spectroscopy (XAS) characterizations. The incorporation of multiple elements is essential for inducing transition metal disorder, which suppresses sodium vacancies and the ordering of electric charges, consequently alleviating interlayer sliding and phase transition of the layer oxide. The capacity of the O3-NFCNTSL cathode retains 81% after 100 cycles at 0.5C. At 2C, a reversible specific capacity of ≈81 mA h g^{-1} can be achieved.

2.3. Understanding the Growth Mechanism of HEO Materials

Gaining insight into the nucleation and growth mechanisms of HEO materials is pivotal for shaping their structure and optimizing their functions. Gao's group investigated the formation dynamics of HEO materials at atomic scale.[45] They utilized

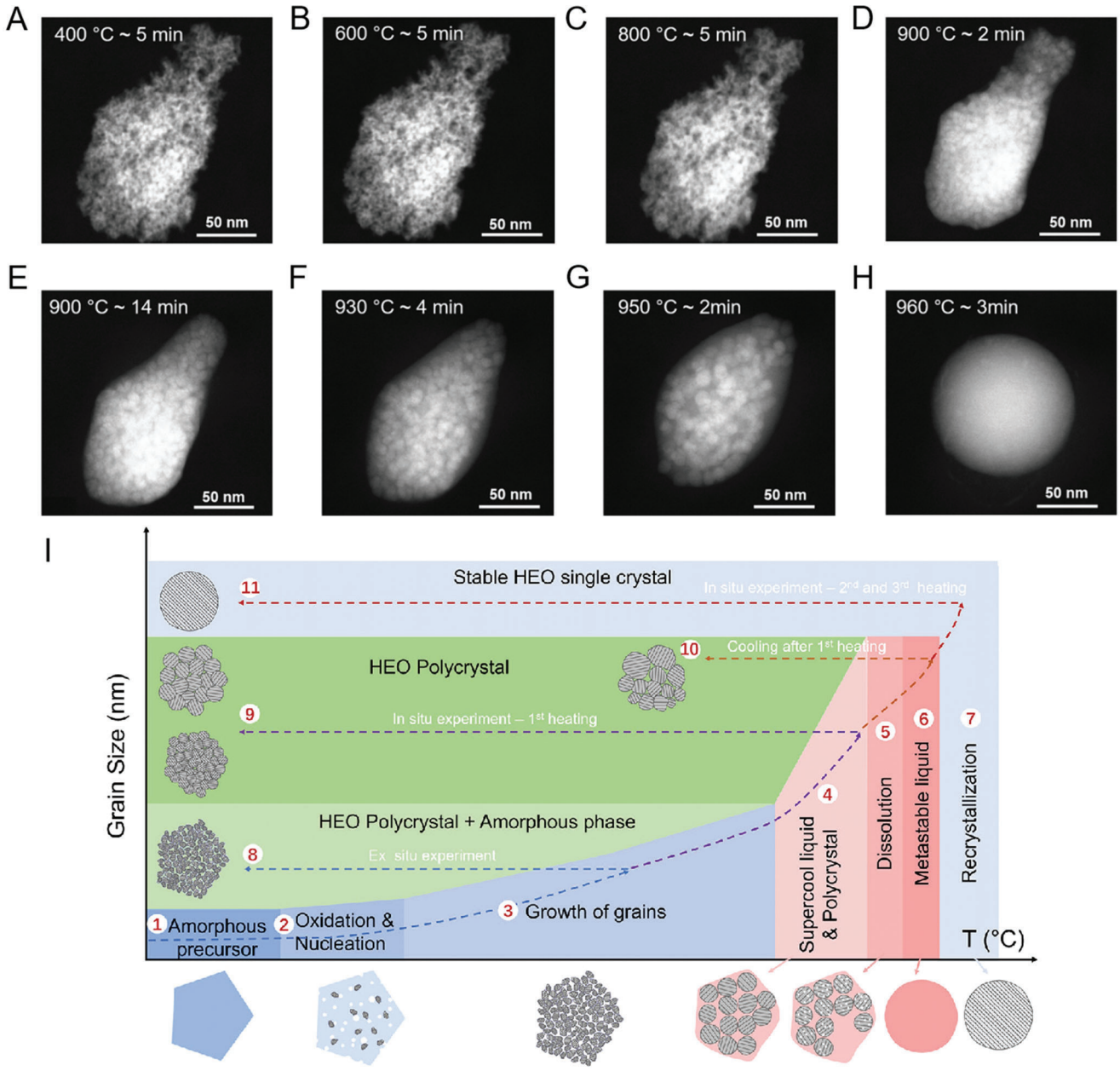

Figure 2. In situ STEM imaging of the HEO evolution during the first heating process using gas cell. A–H) Sequential HAADF STEM images showing the evolution of a cluster of HEO particles during in situ annealing in the formation gas of 20% O_2/80% N_2. I) Schematic of the HEO formation mechanism. With an increase in temperature, the polymetric precursor 1) goes through oxidation and nucleation 2), grain growth 3), the state of supercooled liquid 4), the formation of a liquid phase via dissolution of small particles 5), the formation of a metastable liquid 6), and recrystallization 7). The blue, purple, orange, and red dashed lines show the synthesis processes of a HEO polycrystal with amorphous grain boundaries 8), the degree of supercooling controlled grain growth 9), the formation of HEO polycrystal structure 10), and the formation of a stable HEO single crystal by a recrystallization process at high temperature 11), respectively. Reproduced with permission[45] Copyright 2022, American Chemical Society.

advanced in situ gas-phase scanning transmission electron microscopy with atomic resolution to observe and analyze the complete generation process of a high-entropy fluorite oxide (HEFO) derived from a polymeric precursor. As shown in **Figure** 2A–H, a process of liquid-assisted grain growth in high-entropy fluorite materials is presented. The microstructural transition is evident around 900 °C. Below 800 °C, nanosized pores form and grains grow as the precursor pyrolyzes. At 900 °C, the pores almost disappear, and a liquid phase gradually emerges in the intergranular, accelerating grain growth. Notably, grain growth primarily occurs in the solid state at lower temperatures, while at higher temperatures, the presence of the liquid phase speeds up the process due to enhanced atomic diffusion. The competition between grain growth and melting depends on the annealing temperature. Small grains undergo melting into the liquid phase, resulting in fewer but larger grains. This transition in grain growth

kinetics occurs in HEFO formation. Above 950 °C, a significant part of the particles grows larger, and some nanograins dissolve in the liquid phase. By 960 °C, the particle transforms into a liquid sphere. Moreover, when a liquid sphere is naturally cooled, a nanoparticle consisting of diverse nanograins with varying diameters is obtained.

However, this structure is not thermodynamically stable. When heated above 900 °C, the nanoparticles undergo a transition back into a liquid phase. This melting occurs at the interface between liquid and solid, and small pores form within the grains, leading to grain dissolution in HEFO. This dissolution is associated with the distribution of specific metal cations. Maintaining the HEFO in a liquid state at temperatures exceeding 990 °C, with an extended holding period leads to recrystallization into a single crystal, which is thermodynamically stable. Understanding the dissolution and crystallization processes involves examining changes in free energy, enthalpy, and entropy (Equation 2). The dissolution of local clusters plays a crucial role in HEFO recrystallization, fostering a homogeneous mix of principal elements in the liquid phase, increasing the ΔS_{mix} and making recrystallization thermodynamically preferred. A comprehensive four-stage formation mechanism, encompassing nucleation during precursor oxidation, diffusive grain growth, compositional homogenization, and entropy-driven recrystallization is outlined (Figure 2I). This understanding is critical for tailoring the structure and functions of HEO materials effectively. Moreover, the strategic distribution of elements within the polymeric precursor is pivotal in facilitating oxidation and nucleation at lower temperatures.

3. Exploring Composition-Properties Correlations of HEO Materials

In this segment, we reviewed the progress of unravelling the intricate relationships between composition and properties in HEO materials from both experimental and theoretical perspectives. This journey aims to shed light on how the deliberate manipulation of composition influences their properties, paving the way for innovative advancements in materials engineering.

3.1. An Experiential Perspective

Analyzing the electronic and local structure of various TMs in HEO during sodium ion extraction/insertion provides crucial insights into the charge compensation mechanism. This exploration contributes to a comprehensive understanding of how these materials undergo changes during charge and discharge processes in SIBs, providing valuable insights to optimize high-entropy cathode materials for enhanced performance. In addition to ex situ XAS spectra for studying valence changes during charge and discharge processes, Fourier-transformed extended X-ray absorption fine structure (FT-EXAFS) spectra can further elucidate element-dependent properties. This allows for the observation of short-range local structure evolution for the specific absorbing atom. Wang et al. utilized the FT-EXAFS to learn the local environment changes near Fe, Co, Ni and Ti metals in layered HEO O3–Na($Fe_{0.2}$ $Co_{0.2}Ni_{0.2}Ti_{0.2}Sn_{0.1}Li_{0.1}$)$O_2$ (O3-NFCNTSL) (**Figure** 3A–D).[55] Two major peaks are observed: the first peak (around R ≈ 1.5–1.6 Å) represents the closest oxygen atoms forming the nearest TMO_6 octahedra around the absorbing TM, and the second peak (at R ≈ 2.6 Å) corresponds to the TM-TM_6 hexagonal arrangement in the second coordination shell. The simulated analysis provides structural details, with Ni-O showing the longest bond length and the highest Debye-Waller factors, attributed to the ionic radius and Ni^{2+} ions' activity. Notably, Fe-O exhibits larger R and d values than low-spin Co^{3+}, suggesting a prevalence of high-spin Fe^{3+} in O3-NFCNTSL. The Mössbauer spectrum analysis of the O3-NFCNTSL electrode with iron (Fe) provides valuable insights. Charging to 4.1 V induces asymmetry in the spectrum, indicating the oxidation of Fe^{3+} to Fe^{4+}, affirming its electrochemical activity. Upon discharge, most Fe^{4+} ions are reduced, though incomplete recovery of Fe's electronic structure suggests factors like unreduced Fe^{4+} contributing to initial irreversible capacity and slight lattice distortion induced by Na^+ extraction/insertion. Electrochemically inactive Ti^{4+} and Sn^{4+} play crucial roles in stabilizing the O3 structure, with Ti^{4+} suppressing Fe migration and Sn^{4+} enhancing redox potential through reduced orbital overlap. This effect, coupled with the simultaneous increase in bond ionicity, is expected to enhance the redox potential.[56,57]

More recently, Walczak et al. designed the $NaMn_{0.2}Fe_{0.2}Co_{0.2}Ni_{0.2}Ti_{0.2}O_2$ HEO cathode and comprehensively analyzed its structural, transport, and electrochemical properties.[58] To confirm whether electrons/holes dominate electrical conductivity, a potentiostatic polarization experiment was conducted (Figure 3E). Applying a polarization potential of 100 mV resulted in a gradual decay of current over about 2 hours, reaching a steady-state value indicating a non-ionic conductivity of $1.05 \bullet 10^{-6}$ S cm^{-1}. The total conductivity, determined from an AC impedance response under identical conditions (refer to the inset of Figure 3E), showed a singular, slightly distorted arc, indicative of a total electrical conductivity of $1.09 \bullet 10^{-6}$ S cm^{-1}. This suggests that the electronic/hole component significantly dominated the total electrical conductivity, accounting for around 96% of the total conductivity. Additionally, changes in the valence states of transition metals within $Na_xMn_{0.2}Fe_{0.2}Co_{0.2}Ni_{0.2}Ti_{0.2}O_2$ during cycling are proposed based on synchrotron XAS measurements (Figure 3F). In the pristine layer, manganese displayed a mixture of +2, +3, and +4 valence states. Surface manganese underwent oxidation, while bulk manganese experienced reduction during discharge. The spectra for iron indicated Fe^{3+} in the pristine sample, which oxidized during charging. For cobalt and nickel, Co^{2+} and Co^{3+} coexisted initially, then rapidly oxidized; nickel ions in the bulk oxidized to various states, including Ni^{4+}. While titanium remains electrochemically inactive during cell operation. These findings provide insights into the dynamic valence changes of transition metals during cell operation. Moreover, the O3-P3 phase transition initiates at around x ≈ 0.9 moles of sodium per formula unit, marking a critical point in the material's behavior.

3.2. A Theoretical Perspective

The potential for battery applications is significantly promising with the advancement of high-entropy composites, and the utilization of machine learning plays a vital role in

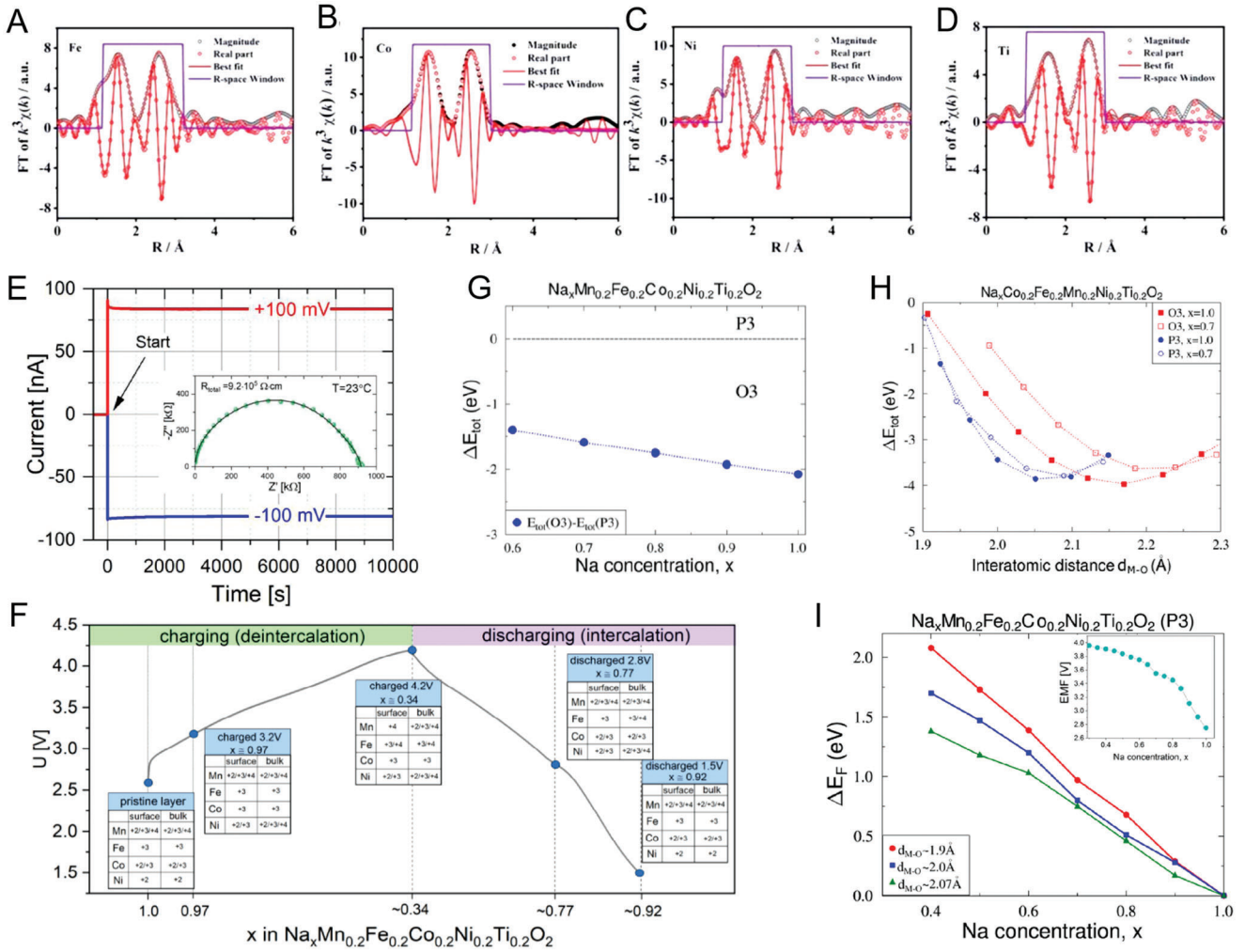

Figure 3. The least-square fits of the calculated FT-EXAFS phase and amplitude functions to the experimental EXAFS spectra for A) Fe, B) Co, C) Ni, and D) Ti in O3-NFCNTSL. Reproduced with permission.[55] Copyright 2022, Royal Society of Chemistry. E) Current response in potentiostatic polarization experiment for $NaMn_{0.2}Fe_{0.2}Co_{0.2}Ni_{0.2}Ti_{0.2}O_2$ layered oxide with ion-blocking Au electrodes at 23 °C. Inset presents a Nyquist plot for the sample measured at the same conditions. F) Changes of valence states of transition metals in $Na_xMn_{0.2}Fe_{0.2}Co_{0.2}Ni_{0.2}Ti_{0.2}O_2$ during charge/discharge processes. G,H) The variation of total energy (Etot) difference versus Na concentration in $Na_xMn_{0.2}Fe_{0.2}Co_{0.2}Ni_{0.2}Ti_{0.2}O_2$ computed by the KKR-CPA method for two structures (O3 and P3) (G); The variation of total energy (Etot) with transition metal M) and oxygen O) distance (dM-O) in O3 and P3 structure $Na_xMn_{0.2}Fe_{0.2}Co_{0.2}Ni_{0.2}Ti_{0.2}O_2$ computed by the KKR-CPA method for x = 1 and x = 0.7 H). I) The variation of the Fermi energy versus Na concentration in P3- $Na_xMn_{0.2}Fe_{0.2}Co_{0.2}Ni_{0.2}Ti_{0.2}O_2$ computed by the KKR-CPA method for different M-O interatomic distances. Inset presents EMF versus Na concentration in $Na|Na^+|Na_xMn_{0.2}Fe_{0.2}Co_{0.2}Ni_{0.2}Ti_{0.2}O_2$ cell. Reproduced with permission.[58] Copyright 2022, Elsevier.

realizing their capabilities. The diversity within high entropy materials opens up various avenues for designing battery materials. However, crafting high entropy materials is a complex process involving multiple factors like element choice, ratio control, and crystal structure. Insights into the elements capable of creating a compatible high-entropy combination through high-throughput modelling are desired to accelerate experimental approaches.[58,59] The traditional trial-and-error and first-principles calculation approaches are time-consuming and inefficient. Therefore, machine learning methods are gaining prominence in accelerating high entropy material development. This data-driven technique leverages existing data to predict material properties and structures, expediting the design process.

Sturman et al. employed a data-driven strategy to identify potential high entropy cathodes for LIBs. They successfully determined the best cathode, $LiN_{i0.2}Mn_{0.2}Co_{0.2}Fe_{0.2}Ti_{0.2}O_2$, which maintained a consistent capacity of 85 mAh g^{-1} during charging up to 4.4 V.[60] In the computational exploration of SIBs, Walczak et al. applied the KKR-CPA method to analyze the electronic structure of high-entropy layered oxide $Na_xMn_{0.2}Fe_{0.2}Co_{0.2}Ni_{0.2}Ti_{0.2}O_2$,[58] specifically focusing on the O3 and P3 crystal structures and their influence on the O3-P3 phase transition (Figure 3G, H). The analyses reveal several key findings: firstly, the O3 phase is energetically favored, influenced by variations in M-O interatomic distances and magnetic interactions among transition metal atoms, which significantly impact the total energy. Notably, iron atoms are active participants

in electron transport within the P3 structure. Moreover, electronic structure differences between the phases are evident, with O3 displaying near half-metallic behavior and strong polarization of electronic states for transition metal atoms. The analysis also indicates that the phase transition has a profound impact on transport properties and electromotive force (EMF) in $Na|Na^+|Na_xMn_{0.2}Fe_{0.2}Co_{0.2}Ni_{0.2}Ti_{0.2}O_2$ cells. Changes in M-O interatomic distances substantially affect the Fermi energy (EF), leading to a broader EF span with shorter distances due to enhanced orbital hybridization. Transitioning to the metallic P3 phase during sodium deintercalation shifts the Fermi level and enhances transport properties (Figure 3I). The observed EMF variations are closely related to changes in the chemical potential of electrons within the cathode material. By applying a semi-empirical model, the study aligns these computational insights with experimental observations, revealing that the O3 phase behaves as a semiconductor, while the P3 phase exhibits metallic characteristics. In essence, this computational analysis provides a comprehensive understanding of how the phase transition impacts EMF, transport behavior, and the transition between semiconductor and metallic features within the HEO $Na_xMn_{0.2}Fe_{0.2}Co_{0.2}Ni_{0.2}Ti_{0.2}O_2$.

While there has been some progress, challenges remain in optimizing HEO materials, especially in terms of optimizing multiple properties and dealing with limited data.[61] Emerging data-driven models like DRXNet offer hope as they can establish connections between cathode composition and electrochemical performance. Successful machine learning applications in future investigations of high entropy compounds require thorough data collection and thoughtful feature engineering.[62,63] As this field continues to evolve, the integration of machine learning in battery research will be closely monitored and further advanced.

4. Merits of HEO Cathodes for Reversible Sodium Storage

High-entropy materials have garnered growing attention in the realm of electrochemical energy storage. In the domain of SIBs, layered transition metal oxides (Na_xTMO_2, $x \leq 1$) are categorized into types like O3, P3, and P2 based on sodium content.[65,66] While O3 layered oxides offer a higher theoretical capacity, they grapple with challenges related to Na^+ resistance and reversibility at elevated voltages. On the contrary, P-type Na_xTMO_2 performs well at high rates due to its superior sodium ion accommodation, reduced phase transition risk, and fast ion diffusion. However, a problematic P-O phase transition during high-voltage charging remains a significant challenge.[67] These challenges have fueled exploration into high-entropy cathodes, featuring multiple components and showcasing superior electrochemical performance with heightened energy density and extended cycling life.[69–71] The subsequent section provides a detailed exploration of the functional roles played by high-entropy design in addressing these challenges.

4.1. Protecting the Structure from Detrimental Phase Changes

Phase transitions in layered materials during cycling can harm battery capacity and cycle life. The issue arises because, during sodiation, the shielding effect between oxygen atoms weakens, resulting in increased spacing between sodium layers. Deep sodium deintercalation transforms the structure of O3-type oxides to the P3 phase, and covalent bonds between transition metals and oxygen are strengthened, but oxygen-oxygen interactions are weakened along with the increase of transition metal valence. This can potentially lead to structural deformation or alkali metal layer collapse. This can potentially lead to structural deformation or alkali metal layer collapse. To address this challenge, researchers are exploring ways to suppress these phase transitions. As early as 2015, introduced a single-phase quinary layer transition metal oxide $NaNi_{1/4}Co_{1/4}Fe_{1/4}Mn_{1/8}Ti_{1/8}O_2$ as a cathode for SIBs. At a 2 C rate, a stable capacity of 96.82 mAh g^{-1} can be achieved after 100 cycles, retaining nearly 97.72% of its initial capacity. The introduction of Ti doping expands the interlayer spacing of the sodium layer, and Mn doping enhances carrier transport properties.[54] This work makes an initial exploration of layered high-entropy materials for SIBs.

Recent research has explicitly shown that a high-entropy strategy effectively prevents detrimental phase changes in layered oxides. Hu's group pioneered the introduction of the high-entropy concept in developing sodium-layered oxides, and they reported an HEO with nine transition metal elements ($NaNi_{0.12}Cu_{0.12}Mg_{0.12}Fe_{0.15}Co_{0.15}Mn_{0.1}Ti_{0.1}Sn_{0.1}Sb_{0.04}O_2$) for SIBs.[25] The nine component ions exhibit varying oxidation states (bivalent to pentavalent) at the octahedral TM site within the O3-$NaTMO_2$ system. These elements, as per existing literature,[72–74] are anticipated to bring about certain potential characteristics: Ni^{2+}, Cu^{2+}, Fe^{3+}, and Co^{3+} are expected to facilitate charge compensation, thereby enhancing capacity. Ti^{4+} and Mg^{2+} play as stabilizers in maintaining the overall structural integrity during Na-(de)intercalation. Mn^{4+} acts as a structure former due to its abundance, while Sb^{5+} and Sn^{4+} contribute to elevating the average voltage. Therefore, this high-entropy approach significantly improved cycling stability, with ≈83% capacity retention after 500 cycles, and improved rate capability, maintaining around 80% capacity retention at a 5 C rate. This improvement is attributed to the highly reversible phase transition between O3 and P3 structures during cycling.

Compared to the conventional O3-type layered materials, an increased reversible capacity of up to ≈60% was found coming from the O3 phase region of the HEO layered counterparts. The researchers proposed a mechanism for how high-entropy compositions support the layered O3-type structure. They used spectral fingerprints to show element types and oxidation states (**Figure 4A, B**). In an HEO cathode, diverse redox elements are randomly distributed, resulting in varied local interactions. During charge–discharge, specific transitional metals change in size and oxidation state, while Na content also fluctuates, impacting local interactions and phase transitions. Traditional cathodes have an even distribution of redox elements, making phase transitions more likely. High-entropy compositions, however, adapt to changes in the diverse local structure. This random arrangement effectively aligns with the unique characteristics of the original structure, postponing phase transitions.

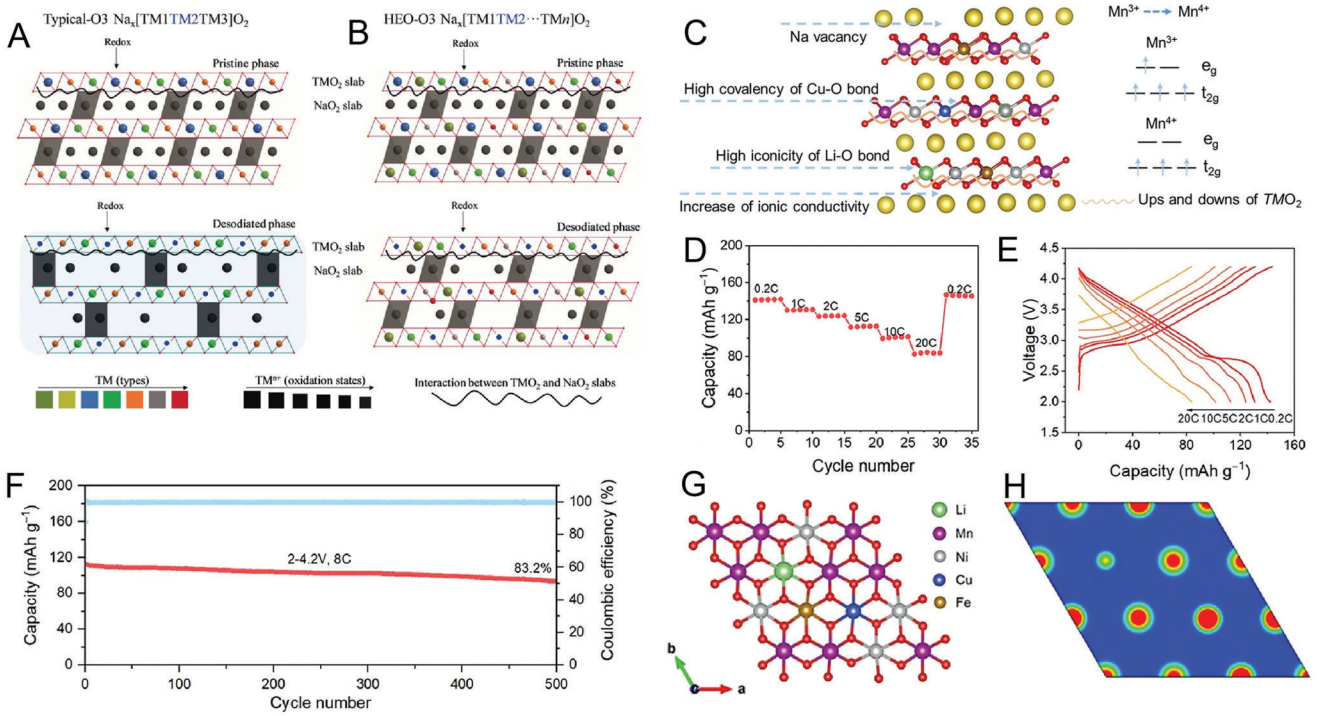

Figure 4. A-B) Possible mechanism of high-entropy composition in facilitating layered O3-type structure. A) The conventional O3-type Na-ion cathodes with three different types TM elements. B) The proposed HEO cathodes with multi-transition-metal element components. TM2 is assigned as the redox element in blue. Note: Two fingerprint spectra are used to illustrate the types and oxidation states of the elements in TM site of O3-type cathodes; the colors represent the types of different TM elements and the sizes represent the different oxidation states where the lower the oxidation state the larger the size of the element. The wavy lines give the local interaction between the elements in TM site and Na in TMO_2 slabs and NaO_2 slabs, respectively. Reproduced with permission.[25] Copyright 2020, Wiley-VCH. C) a Schematic of O3-type $Na_{0.95}$LNCFM structure design. D,E) Rate performance. F) Long-term cycling performance at 8C rate. G) Schematic structures of Na0.95LNCFM. H) Contour maps of charge density on corresponding planes in $Na_{0.95}$LNCFM. Reproduced with permission.[68] Copyright 2023, Springer Nature.

Chen and his colleagues further confirmed this conclusion.[75] A high-entropy O3-type layer-structured material with non-equimolar components, $NaCu_{0.1}Ni_{0.3}Fe_{0.2}Mn_{0.2}Ti_{0.2}O_2$ (NCNFMT), was fabricated, establishing as a cathode for SIBs. Significantly, in situ synchrotron X-ray diffraction unequivocally studied the reaction mechanism, indicating that the phase transition was postponed until the removal of 0.32 sodium ions from NCNFMT, underscoring the stabilization of the O3-phase facilitated by the high entropy effect. However, further in-depth research is required to explore the feasibility of retarding or accelerating the phase transition in high-entropy structures. The composition of the high-entropy NCNFMT with various element ratios was investigated as well. This study confirmed that certain elements, such as Mn^{4+} and Ti^{4+}, remain inactive during cycling, which aids in maintaining structural stability. Meanwhile, the presence of Ni^{2+} and Cu^{2+} ions increases both capacity and potential. Additionally, Co^{3+} helps relieve the Jahn-Teller effect of Mn^{3+}, further enhancing the structural stability of HEO materials.

Very recently, a high-entropy design, incorporating a Li doping strategy, was introduced for $Na_{0.95}Li_{0.06}Ni_{0.25}Cu_{0.05}Fe_{0.15}Mn_{0.49}O_2$ ($Na_{0.95}$LNCFM) (Figure 4C).[68] This innovative approach aims to alleviate lattice stress and boost ionic conductivity. The cathode not only showcases outstanding rate capability, achieving a discharge capacity of 85 mAh g^{-1} even at 20 C, but also exhibits remarkable long-term stability, retaining 83.2% of its capacity after 500 cycles at 8C (Figure 4D–F). These exceptional electrochemical characteristics are attributed to the swift and reversible O3-P3 phase transition in low-voltage regions, effectively suppressing phase transitions. Moreover, the $Na_{0.95}$LNCFM electrode behaves highly stable in air and heat. DFT calculations revealed that by replacing Li^+ ions with slightly larger Na^+ ions, the weaker Li-O orbital hybridization was achieved, promoting efficient charge transfer from sodium to oxygen (Figure 4G,H). This resulted in a stronger Na-O binding energy, reducing the risk of active Na loss and preventing irreversible phase transitions during air exposure. Additionally, the higher redox potential of Cu^{2+} made it more resistant to oxidation in air, preventing the chemical extraction of Na^+ from the lattice.

The high-entropy design also can stabilize the P2-type layered oxide cathodes. Liu and co-authors underscored the importance of the entropy stabilization concept in battery cycling by comparing the electrochemical performance of P2-type medium-entropy 3-cation oxide (1.28 R) and 4-cation oxide (1.28 R) under the same testing conditions.[81] Their research indicated that a rise in configurational entropy led to smoother charge–discharge profiles. Furthermore, it bolstered the stability of the crystal structure and mitigated the complex

phase transitions of Mn^{3+} during the continuous Na intercalation/delamination process. The outcomes presented above indicate that the presence of a high entropy structure in the layered material can efficiently inhibit the typical monoclinic phase transition observed in both O3- and P2-type layered materials, thereby enhancing the stability of the structure during cycling processes.

4.2. Facilitating the Reaction Kinetics

An early investigation into P2-type high-entropy oxides was conducted by Yang and their team.[80] They crafted a P2-type high-entropy oxide, $Na_{0.6}Ti_{0.2}Mn_{0.2}Co_{0.2}Ni_{0.2}Ru_{0.2}O_2$, using a solid-phase method. This high-entropy cathode stands out with smoother charge/discharge curves, indicating reduced resistance during Na^+ ion movement. The researchers suggest that various high-entropy components in the transition metal layer disrupt cation and charge ordering, making it easier for sodium to diffuse. Conversely, non-high-entropy layered materials tend to have ordered transition metal arrangements, leading to higher diffusion barriers for Na^+ ions. The high-entropy cathode achieves discharge capacities of 78 and 68 mAh g^{-1}, even at 10 and 15 A g^{-1}, respectively. Moreover, Monte Carlo simulations were utilized to evaluate the impact of various transition metal elements on Na^+ ion migration barriers (**Figure 5A**). They found that $Na(f)_{Ni\text{-}Ni}$ sites had the lowest barrier to Na^+ ion migration, with $Na(f)_{Ni\text{-}Co}$ and $Na(f)_{Co\text{-}Co}$ sites ranking next. Ti and Mn showed intermediate migration barriers, while Ru presented the highest barrier. x Additionally, they defined the element ratio needed for swift Na^+ ion diffusion in the P2 structure. To support rapid charging and discharging, Ru, a significant hindrance to the migration of sodium ions, should be present at less than 0.293, while elements favoring sodium migration should exceed 0.293. This initiative study provides valuable insights for future research on P2-type layered cathode materials. Similar boosted electrochemical reaction kinetics and enhanced performance were witnessed in HEO cathodes with different chemical formulas, such as $Na_{0.75}Mn_{0.5625}Ni_{0.25}Cu_{0.0625}Mg_{0.0625}Ti_{0.0625}O_2$ and $Na_{0.67}Ni_{0.18}yCu_{0.1}Zn_{0.05}Fe_xMn_{0.67\text{-}x+y}O_2$.[19,20]

Ji et al. manipulated configurational entropy by adjusting the stoichiometric ratio of inactive cations (Mn^{4+}, Ti^{4+}) and investigated the entropy contributions to performance in Na-deficient O3-type layered HEOs cathode, $Na_{0.83}Li_{0.1}Ni_{0.25}Co_{0.2}Mn_xTi_xSn_{0.45-2x}O_{2-\delta}$ (MTS45, x = 0; MTS35, x = 0.05; MTS25, x = 0.1; MTS15, x = 0.15).[82] The theoretical configurational entropy (S_{conf}) values gradually increase per unit cell for the MTS45, MTS35, MTS25, and MTS15 cathodes. (Figure 5B) In-depth electronic structure analysis (Figure 5C) revealed heightened electron localization between O and Ti in MTS15 compared to MTS45. This concentrated electron density weakened the Na—O bond, facilitating Na^+ diffusion by reducing electrostatic interaction with interlaminar sodium ions. To gain a deeper understanding of the exceptional entropy-driven kinetics of Na^+ diffusion, the activation energy (E_a) was derived through EIS analysis at varying temperatures. (Figure 5D, E) According to the Arrhenius equation, depicted in the inset of Figure 5F, the diffusion energy barrier of MTS15 is effectively relieved.

4.3. Regulating the Crystal Structure of Oxides

An optimized crystal structure could provide capacious channels for rapid ion migration and protect the structure integrity from degradation, thereby contributing to enhanced performance. Understanding the interplay between entropy and anionic redox kinetics within the crystal structure of layered cathodes, especially under high voltage, offers a promising avenue for developing layered cathodes with both rapid charging and extended cycle life. Xu et al. put forth the idea that the surface energy of P2-type entropy-tuned materials, exemplified by $Na_{0.62}Mn_{0.67}Ni_{0.23}Cu_{0.05}Mg_{0.07}Ti_{0.01}O_2$ (CuMgTi-571), is primarily shaped by configurational entropy (S_{config}) at specific temperatures.[84] This suggests that variations in S_{config} can effectively modify the surface energy of crystal planes, impacting the growth rate of distinct facets. Their study showcases that high configurational entropy acts as the driving force for the growth of a significant percentage of {010} active facets in layered cathodes, as illustrated in Figure 5G–I. The CuMgTi-571-based positive electrode exhibits impressive performance, boasting 87% capacity retention after 500 cycles at 120 mA g^{-1} and ≈ 75% capacity retention after 2000 cycles at 1.2 A g^{-1}. These results highlight the potential of entropy-tuned materials to address structural issues associated with high-voltage operations, providing a promising avenue for advanced battery technology, while also emphasizing the significant impact of configurational entropy on surface energy and facet growth rates.

4.4. Tailoring Electronic Structure of Oxides

Recently, Hu and colleagues demonstrated that the incorporation of strategic low-valence cation in HEO composition can maximize high-voltage TM redox reactions, tailoring the electronic structure by increasing the Na^+/TM charge transfer ratio.[85] Substituting Li^+ for $Na_xCu_{0.11}N_{i0.11}Fe_{0.3}Mn_{0.48}O_2$ (CNFM, LCNFM) boosts this ratio, facilitating high-voltage TM redox activity. Additionally, F co-substitution stabilizes the crystal structure, resulting in $Na_{0.89}Li_{0.05}Cu_{0.11}Ni_{0.11}Fe_{0.3}Mn_{0.43}O_{1.97}F_{0.03}$ (LCNFMF). In-depth DFT calculations on Na-Cu-Fe-Mn-O oxide material and Li-substituted versions revealed Cu and Fe 3d band centers overlapping Mn at a lower energy level, indicating higher redox potential. In CNFM, the Mn 3d band near the Fermi level suggests $Mn^{3+/4+}$ redox upon Na^+ removal. Li-substituted samples show a positive shift in Mn d projected density of states (PDOS), indicating Mn ion oxidation and improved charge balancing, resulting in a narrower band gap compared to CNFM (**Figure 6A**). Despite similar initial Na^+ content, CNFM experiences Na^+ loss and Mn ion oxidation due to the Fermi level residing in Mn 3d orbitals. Conversely, in LCNFM, controlled low-valence cation substitution optimizes the Na^+ content to the average coordination number (ACTN) of TMs, promoting TM redox reactions for maximal capacity contribution (Figure 6B).

Initial charge-discharge curves reveal increased charge capacities with Li substitution, attributed to improved high-voltage TM oxidation reactions (Figure 6C). The high-entropy LCNFMF cathode exhibits a ~29% capacity increase from high-voltage TMs and outstanding extended cycling durability due to enhanced structural reversibility. Analyzing the Na^+ to TM coordination ratios

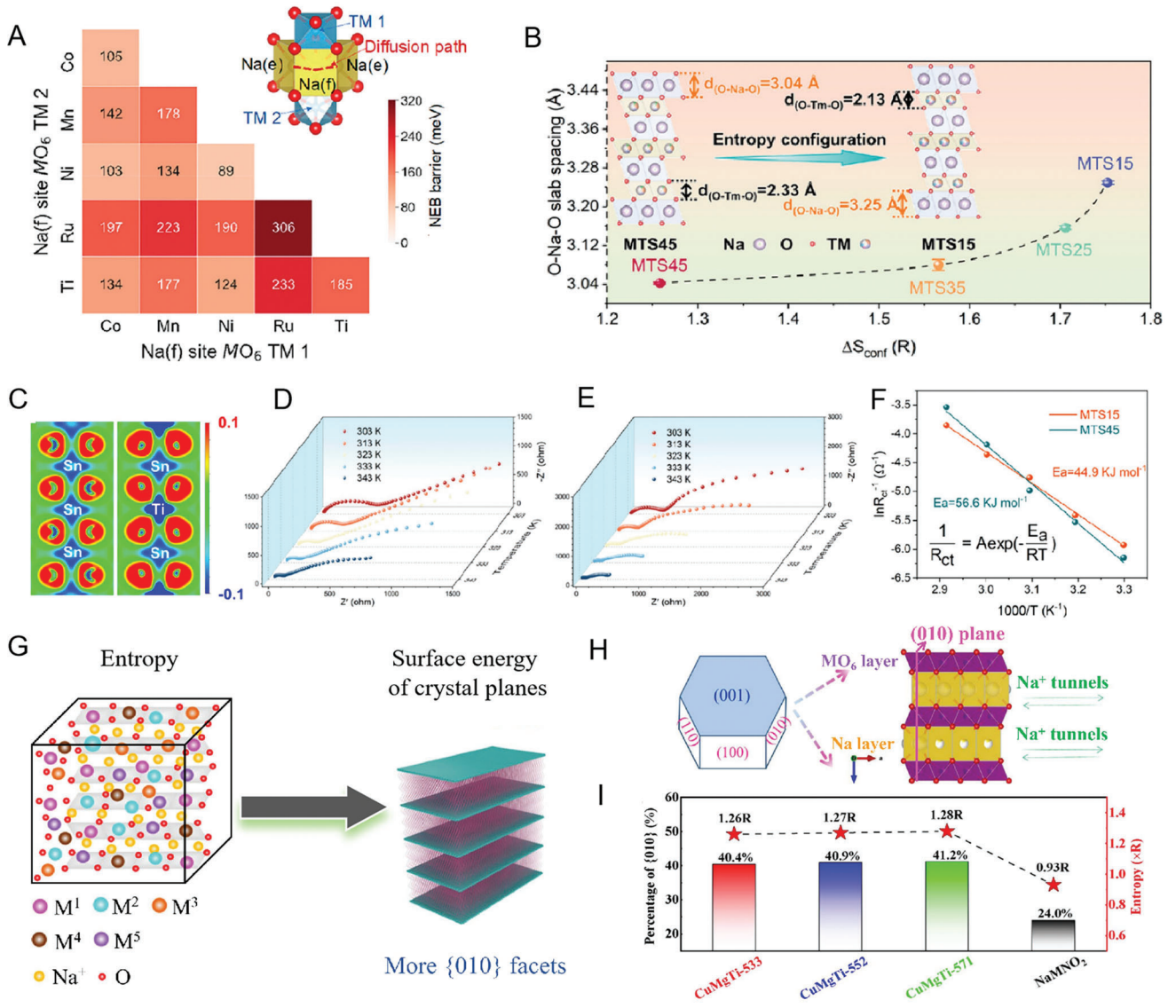

Figure 5. A) Na(e)−Na(f)−Na(e) single Na hopping migration barriers (meV) of different Na(f) site compositions at the fully charged limit. Reproduced with permission.[80] Copyright 2022, American Chemical Society. B) Variation trends between configurational entropy (S_{conf}) and the O–Na–O slab spacing. C) 2D slices of the charge density distribution for MTS45 (left) and MTS15 (right). D,E) electrochemical impedance spectroscopy (EIS) spectra of the electrodes at the fully discharged state after 10 cycles. F) Arrhenius curve for the R_{ct} and activation energy of the MTS15 and MTS45 cathodes. Reproduced with permission.[82] Copyright 2023, American Chemical Society. G) Schematic illustration of microparticles with six {010} facets and two {001} facets. The surface atomic arrangement of (010) facet is shown on the right. H) Schematic illustration of microparticles with six {010} facets and two {001} facets. The surface atomic arrangement of (010) facet is shown on the right. I) The percentage of {010} facets and configurational entropy of CuMgTi-533, CuMgTi-552, CuMgTi-571, and $NaMNO_2$ samples. Reproduced with permission.[84] Copyright 2022, Springer Nature.

in Mn-based Na-ion layered oxide cathodes reveals redox mechanisms and the impact on electronic structure (see Figure 6D). When the ratio is around or marginally above 1, conventional cationic redox, involving high-voltage TMs, dominates charge storage. In cases of Na^+ deficiency, discharge triggers low-voltage Mn reduction with extra Na^+ intercalation, evident in the downward shift of Mn 3d orbitals. Conversely, when all Na crystallographic sites are filled, there is no increase in capacity gain from additional Mn redox due to the limit of Na^+ intercalation. With a significantly higher ratio, oxygen redox is activated as the O 2p state energy rises towards the Fermi level. In scenarios where the ratio tends to infinity, only oxygen redox occurs because there are no available electrons from the TMs to facilitate Na^+ deintercalation. This encourages involvement in electrochemistry with increased energy levels of the O 2p states.

4.5. Alleviating the Jahn-Teller Distortion and Enhancing Oxygen Reversibility upon Cycling

The dominance of Ni and/or Mn as transition metal elements in layered oxides introduces structural distortion because of the

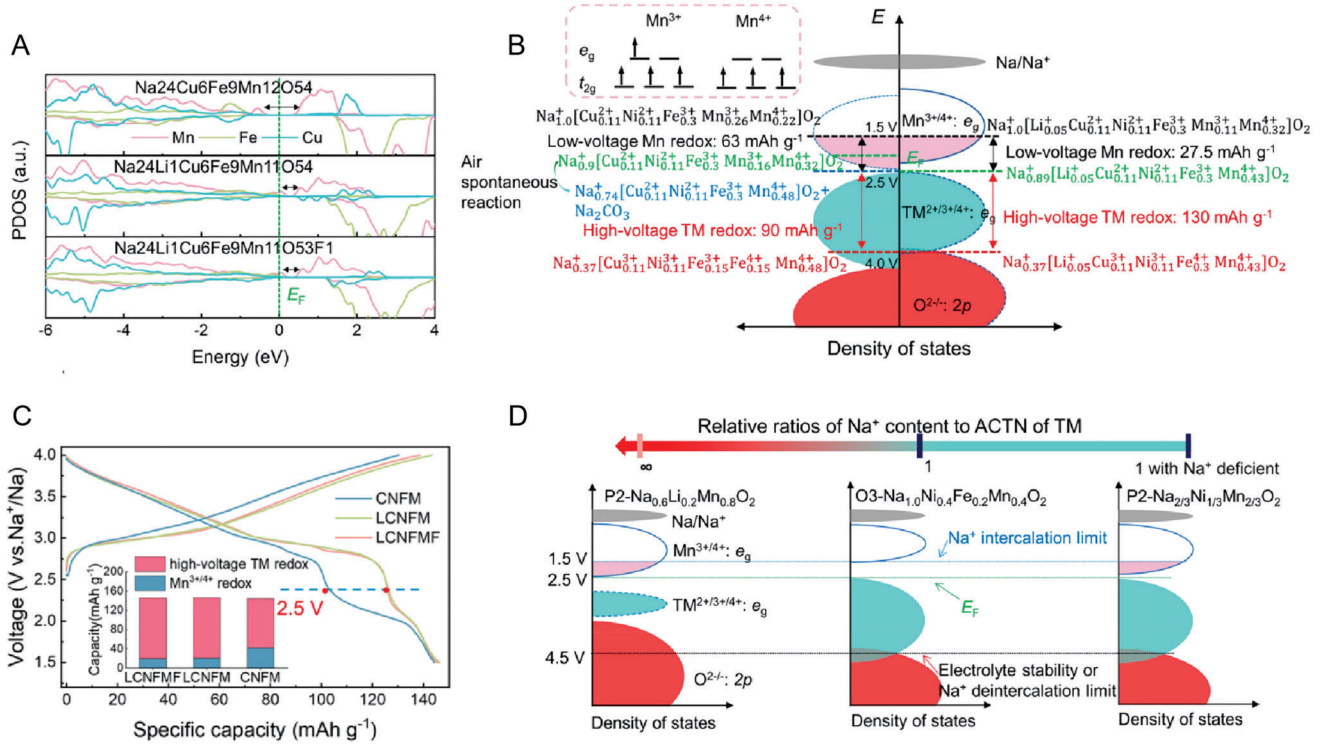

Figure 6. A) Calculated projected density of states of TMs for $Na_{24}Cu_6Fe_9Mn_{12}O_{54}$, $Na_{24}Li_1Cu_6Fe_9Mn_{11}O_{54}$, and $Na_{24}Li_1Cu_6Fe_9Mn_{11}O_{53}F_1$. B) Schematic illustration of the electronic structure adjustment of CNFM and LCNFM, E_F: Fermi level. Dotted box: the electron occupancy in 3d orbitals of Mn^{3+} and Mn^{4+}. C) Initial charge-discharge curves of CNFM, LCNFM, and LCNFMF at 0.1 C in a voltage range of 1.5–4.0 V. Inset: quantitative analysis results of the reversible capacity contributions. D) Schematic band structure of typical Na layered oxides. Reproduced with permission [85] Copyright 2023, American Chemical Society.

Jahn-Teller effects of high-spin Mn^{3+} and Ni^{3+}, leading to electrode instability. Besides, the poor oxygen redox reversibility at high voltages compromises oxide structural integrity, negatively impacting SIB performance. Recent works in HEO cathodes have proven that the high-entropy design could effectively address these challenges and benefit the structural stability of layer oxides.

Hu's group introduced a high-entropy configuration into O3-$NaNi_{0.4}Fe_{0.2}Mn_{0.4}O_2$ (NFM424) base cathode material, synthesizing $NaNi_{0.25}Mg_{0.05}Cu_{0.1}Fe_{0.2}Mn_{0.2}Ti_{0.1}Sn_{0.1}O_2$ (HEO424).[76] HEO424 achieved balance by offering charge compensation (Cu^{2+}), structural stability (Mg^{2+} and Ti^{4+}), and increased average voltage (Sn^{4+}). Moreover, the expanded TMO_2 slabs of HEO424 compared to NFM424 during the initial charging process (**Figure 7A**) may alleviate the Jahn–Teller distortion of the Ni^{3+} active center and favor high-symmetry structures.[77] Thereby, it maintained a pure O3-type phase, enabling fast Na^+ transport and ensuring structural integrity during cycling, even with improved thermal safety properties.

Combining high-entropy design with superlattice stabilization offers a strategy to prolong cycle life and improve the rate capability of layered cathodes. Illustrated by high-entropy $Na_{2/3}Li_{1/6}Fe_{1/6}Co_{1/6}Ni_{1/6}Mn_{1/3}O_2$ cathode, this approach showcases a superlattice structure with ordered Li/transition metals.[78] Notably, this cathode displays outstanding electrochemical performance, remaining unaffected by phase transitions and oxygen redox during cycling (Figure 7B–D). The cathode retains 63.7% of its capacity at 5 C after 300 cycles and demonstrates a rapid-charging capability of 78 mAh g^{-1} at 10 C. EXAFS experiments were conducted to verify the electrochemically active/inert ions and gain insights into the alteration of the local ligand environment in NaLFCNM (Figure 7E). A notable reduction in interatomic distance is identified at Ni and Fe K-edges during charging, indicating the oxidation of Ni and Fe ions. Conversely, the Co and Mn K-edges exhibit minimal changes during Na removal from the crystal lattice, which avoids the Jahn-Teller effects and stabilizes the electrode structure (Figure 7F).

5. Applications of HEO Materials for SIBs

5.1. Overview of the Development of P2 or O3 Layered HEO Cathodes

Thanks to the merits of the high entropy design discussed above, HEOs stand out as promising contenders as cathodes for sustainable SIBs. This prominence arises from their straightforward fabrication process and robust structural compatibility, enabling efficient reversible Na^+ (de)intercalation chemistry.[64,86] **Table 1** summarizes the battery performance of various O3 and P2 layered cathodes with high-entropy configurations in SIBs. It's worth mentioning that Ni is a common constituent in all of the layered oxides listed in the table, serving as an active redox center with the potential advantage of

Table 1. Summary of O3 and P2 Layered Cathodes with High-Entropy Configurations in SIBs.

Cathode	Voltage range [v]	Initial Capacity [mAh g^{-1}]	Cycle retention	Rate performance [mAh g^{-1}]	Reference
P2-$Na_{0.67}Ni_{0.165}Cu_{0.1}Zn_{0.05}Fe_{0.03}Mn_{0.655}O_2$	2.5–4.4	105	92.7% after 200 cycles/ 1C	77.49/ 5 C	[19]
P2-$Na_{0.75}Mn_{0.5625}Ni_{0.25}Cu_{0.0625}Mg_{0.0625}Ti_{0.0625}O_2$	2.0–4.3	108	97.2% after 100 cycles	/	[20]
O3-$NaNi_{0.12}Cu_{0.12}Mg_{0.12}Fe_{0.15}Co_{0.15}Mn_{0.1}Ti_{0.1}Sn_{0.1}Sb_{0.04}O_2$	2.0–3.9	110	83% after 500 cycles/ 3C	86/ 5C	[25]
O3-$NaNi_{1/4}Co_{1/4}Fe_{1/4}Mn_{1/8}Ti_{1/8}O_2$	2.0–4.0	128	97.72% after 100 cycles/ 2C	38.6/ 60C	[54]
O3-$NaFe_{0.2}Co_{0.2}Ni_{0.2}Ti_{0.2}Sn_{0.1}Li_{0.1}O_2$	2.0–4.2	130.6	72% after 100 cycles/ 0.1C	80.8/ 2 C	[55]
O3-Na $Mn_{0.2}Fe_{0.2}Co_{0.2}$ $Ni_{0.2}Ti_{0.2}O_2$	1.5–4.2	180	97% after 100 cycles/ 0.1C	173/ 5 C	[58]
$Na_{0.95}Li_{0.06}Ni_{0.25}Cu_{0.05}Fe_{0.15}Mn_{0.49}O_2$	2.0–4.2	141.2	83.2% after 500 cycles/ 8 C	85/ 20C	[68]
O3-$NaCu_{0.1}Ni_{0.3}Fe_{0.2}Mn_{0.2}Ti_{0.2}O_2$	2.0–3.9	130	87% after 100 cycles/ 0.1C	85/ 5 C	[75]
O3-$NaNi_{0.25}Mg_{0.05}Cu_{0.1}Fe_{0.2}Mn_{0.2}Ti_{0.1}Sn_{0.1}O_2$	2.0–4.0	130.8	75% after 500 cycles/ 1C	108/ 5C	[76]
O3-$Na_{2/3}Li_{1/6}Fe_{1/6}Co_{1/6}Ni_{1/6}Mn_{1/3}O_2$	2.0–4.5	171.2	89.3% after 90 cycles / 1C	78/ 10C	[78]
O3-$Na_{0.8}Ni_{0.2}Fe_{0.2}Co_{0.2}Mn_{0.2}Ti_{0.2}O_2$	2.0–4.0	107	90% after 100 cycles/ 0.05C	94.1/ 5 C	[79]
P2-$Na_{0.6}(Ti_{0.2}Mn_{0.2}Co_{0.2}Ni_{0.2}Ru_{0.2})O_2$	1.5–4.5	174	40.9% after 400 cycles/ 0.1C	68/ 86C	[80]
$Na_{0.83}Li_{0.1}Ni_{0.25}Co_{0.2}Mn_{0.15}Ti_{0.15}Sn_{0.15}O_{2-\delta}$	2.0–4.2	109.4	87.2% after 200 cycles/ 2C	83.3/ 10C	[82]
$Na_{0.95}Li_{0.07}Cu_{0.11}Ni_{0.11}Fe_{0.3}Mn_{0.41}O_{1.97}F_{0.03}$	1.5–4.0 V	138.6	73.1% after 302 cycles/ 1C	109/ 10C	[85]
P2-$Na_{0.79}Li_{0.13}Ni_{0.20}SS_{0.01}Mn_{0.66}O_2$ (LNSM-0.01)	2.0–4.5	~160	93.27% after 100 cycles/ 0.5C	85.7/ 7C	[88]
O3/P2-$Na_{0.85}Li_{0.05}Ni_{0.25}Cu_{0.025}Mg_{0.025}Fe_{0.05}Al_{0.05}Mn_{0.5}Ti_{0.05}O_2$	2.0–4.2	122	88% after 300 cycles/ 2C	81.8/ 10C	[89]
O3-$Na(Fe_{0.2}Cu_{0.1}Ni_{0.2}Mn_{0.3}Ti_{0.2})O_2$	2.0–4.1	121	83.8% after 200 cycles/ 2C	70.2/ 5C	[90]
P2/O3-$Na_{0.7}Mn_{0.4}Ni_{0.3}Cu_{0.1}Fe_{0.1}Ti_{0.1}O_{1.95}F_{0.1}$	2.0–4.3	118.4	88.9% after 200 cycles/ 2C	108.5/ 2C	[91]
O3- $NaNi_{0.3}Cu_{0.1}Fe_{0.2}Mn_{0.2}Ti_{0.2}O_2$	2.0–4.0	123.6	77.2% after 200 cycles / 0.1C	110.0/ 0.5C	[92]
O3- $NaMn_{0.2}Fe_{0.2}Co_{0.2}Ni_{0.2}Sn_{0.1}Al_{0.05}Mg_{0.05}O_2$	1.5–4.2	152	71.1% after 200 cycles/ 0.5C	142/ 0.5C	[93]
O3-$Na_{0.95}Li_{0.06}Ni_{0.25}Cu_{0.05}Fe_{0.15}Mn_{0.49}O_2$	2.0–4.2	141.2	88% after 200 cycles/ 2C	112.6/ 5C	[94]
P2-$Na_{0.667}Mn_{0.667}Ni_{0.167}Co_{0.117}Ti_{0.01}Mg_{0.01}Cu_{0.01}Mo_{0.01}Nb_{0.01}O_2$	1.5–4.5	169.8	76.4% after 100 cycles/ 1C	111/ 5C	[95]
O3-$NaNi_{0.1}Mn_{0.15}Co_{0.2}Cu_{0.1}Fe_{0.1}Li_{0.1}Ti_{0.15}Sn_{0.1}O_2$	2.0–4.1	115	82.7% after 1000 cycles / 16C	~100/ 8C	[96]
P2-$Na_{0.67}(Mn_{0.45}Ni_{0.18}Co_{0.18}Ti_{0.1}Mg_{0.03}Al_{0.04}Fe_{0.02})O_2$	2.6–4.6	102	86% after 50 cycles /0.5C	/	[97]
O3-$Na_{0.94}Ni_{0.29}Cu_{0.1}Fe_{0.16}Mn_{0.3}Ti_{0.15}O_2$	2.0–4.0	122	79% after 300 cycles/ 0.5	68/ 4 C	[98]
P2-$Na_{0.75}Mn_{0.55}Ni_{0.25}Co_{0.05}Fe_{0.10}Zr_{0.05}O_2$	1.5–4.2	143	81% after 100 cycles/ 0.1C	22/ 10 C	[99]

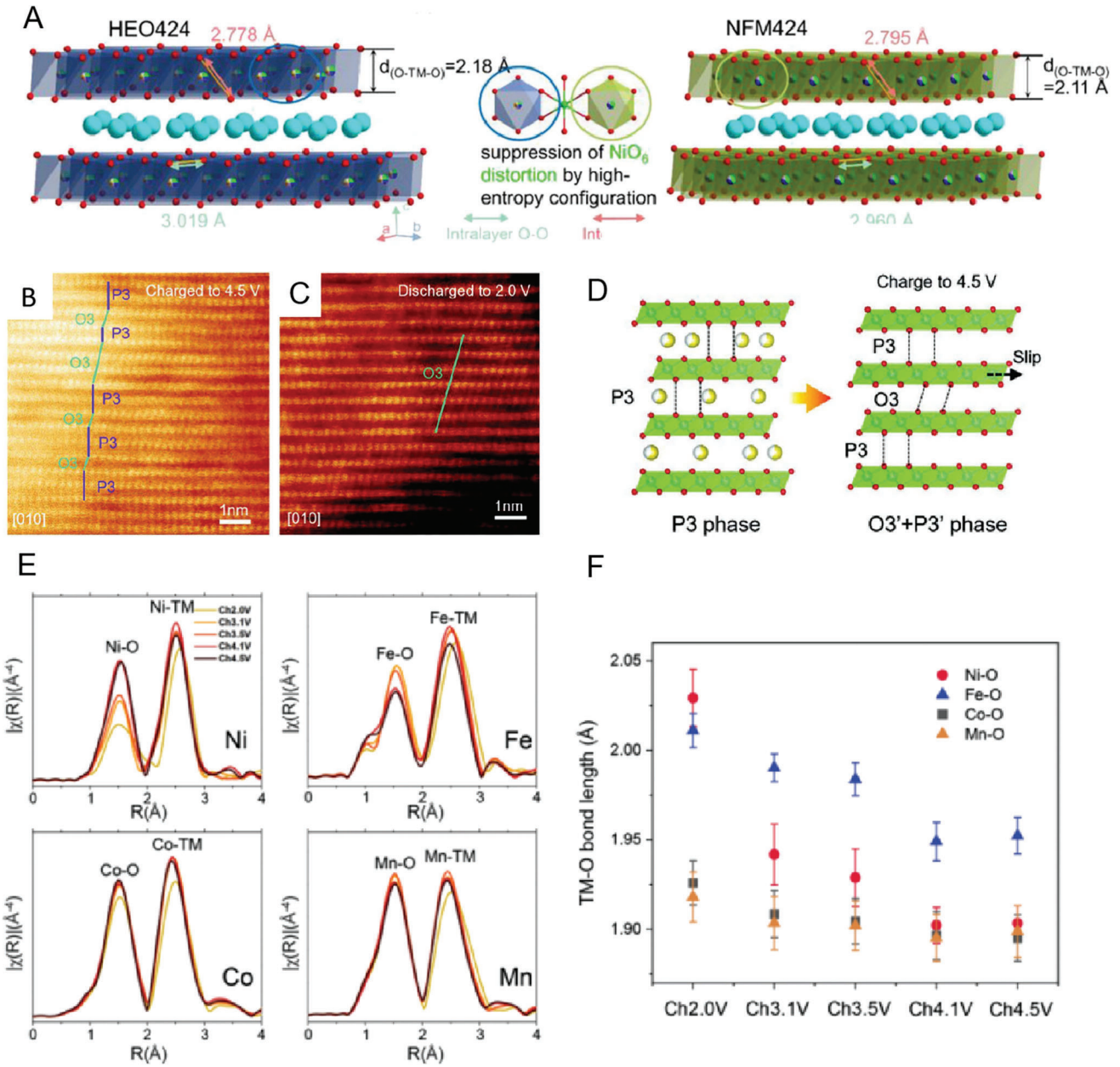

Figure 7. A) Schematic illustrations showing the TMO_2 slabs in both cathodes during the initial charge process. Reproduced with permission [76] Copyright 2022, American Chemical Society. B,C) Ex situ HR-TEM image of NaLFCNM at B) 4.5 V state and C) 2 V state. D) Schematic illustrations of the whole phase evolution of NaLFCNM upon charge and discharge. E) EXAFS spectra of Ni k-edge, Fe k-edge, Co k-edge, and Mn k-edge. F) The TM-O (TM = Ni, Fe, Co, and Mn) bond length changes upon charging from 2.0 to 4.5 V. Reproduced with permission[78] Copyright 2022, Wiley-VCH.

offering higher voltage. Moreover, Fe/Mn/Ti is frequently employed in high-entropy-based layered oxides as well. Research on high-entropy layered oxides in SIBs covers both O3 and P2 phases, with a preference for O3 because of their higher specific capacities and potential for more considerable performance improvement.

For example, Anang and Walczak both pioneered HEO cathodes for SIBs, introducing compositions like $Na_{0.8}Ni_{0.2}Fe_{0.2}Co_{0.2}Mn_{0.2}Ti_{0.2}O_2$ and $NaNi_{0.2}Fe_{0.2}Co_{0.2}Mn_{0.2}Ti_{0.2}O_2$, respectively. These cathode materials exhibit a reversible O3-P3-O3 phase transition during cycling.[58,79] Walczak et al. suggest that the transition from O3 to P3 phases could be associated with magnetic interactions within high-entropy structures. Through operando-XRD tests, the material was observed undergoing an O3-P3 phase transition at a sodium content (x) of 0.9. This rapid phase transition results in a low sodium diffusion coefficient and excellent metal conductivity, elucidating the material's high capacity and rate capability. They propose that high-entropy layered oxide, with lower cobalt and nickel content, could be suitable for sodium battery technology,

particularly in large-scale energy storage systems. In a similar vein, Tian and colleagues also investigated an O3-type layered high-entropy oxide, $Na(Fe_{0.2}Co_{0.2}Ni_{0.2}Ti_{0.2}Sn_{0.1}Li_{0.1})O_2$, where a reversible O3-P3-O3 phase transition process was evidenced in this system.[55]

The preceding materials demonstrate that a high-entropy structure in layered materials can efficiently inhibit the typical monoclinic phase transition found in O3-type layered materials, enhancing the stability of the structure during sodiation/desodiation. However, the relatively low ICE caused by initial capacity loss still hinders the practical application of HEOs.[60] Chen's work may help explain the underpinning mechanisms.[87] During the initial charging process, they discovered the generation of an M_3O_4 phase on the surface of equimolar high-entropy layered oxide $LiNi_{0.2}Mn_{0.2}Co_{0.2}Fe_{0.2}Al_{0.2}O_2$. This surface phase obstructs the re-intercalation of lithium ions in subsequent cycles. Metal ion migration involves Ni^{2+} passing from octahedral to tetrahedral sites, while reduced Fe^{2+} and Co^{2+} migrate directly to tetrahedral 8a sites, forming the M_3O_4 phase. As more Fe^{3+} and Co^{3+} are reduced, more irreversible M_3O_4 is formed, which should be suppressed to achieve high-performance cathode materials.

5.2. P2/O3 Biphasic HEO Cathodes

The high-entropy design was also adopted together with the phase engineering to reinforce the robustness of layered oxide cathodes. Cheng et al. developed a high-entropy cathode material, $Na_{0.7}Mn_{0.4}Ni_{0.3}Cu_{0.1}Fe_{0.1}Ti_{0.1}O_{1.95}F_{0.1}$ (P2/O3-NaMnNiCuFeTiOF), with a tunable P2/O3 biphasic structure.[83] In situ XRD analysis during synthesis at various sintering temperatures revealed the generation process's sensitivity to temperature, showcasing the tunable P2/O3 biphasic structure (**Figure 8A**). At 500 °C, a pure P3 phase forms, transitioning to the P2/O3 biphasic structure at temperatures exceeding 640 °C. The P2/O3 ratio within the biphasic structure changes with sintering temperature. HRTEM confirms the presence of the biphasic P2/O3 at the phase boundary (Figure 8B). The P2/O3-NaMnNiCuFeTiOF cathode demonstrates a high initial Coulombic efficiency (97.6% at 20 mA g^{-1}), substantial capacity retention across a broad temperature range (−40 – 50 °C), and extended storage stability (90 days). The outstanding Na-storage performance is credited to the engineered high-entropy and biphasic structure, which enhances structural stability by alleviating Jahn-Teller distortion and preventing the sliding of transition metal layers over a broad temperature range (Figure 8C).

5.3. Gradient HEO Cathodes

Very recently, Li et al. pioneered a unique methodology utilizing steel slag for multi-element gradient doping, introducing SS (the SS includes numerous available elements, like Fe, Ca, Mg, Si, Li and Mn) into P2-type layered oxides ($Na_{0.79}Li_{0.13}Ni_{0.20}SS_xMn_{0.67-x}O_2$, x = 0, 0.005, 0.01, 0.03) (Figure 8D).[88] The high-entropy cathode materials (HECMs) exhibit outstanding capacity retention, maintaining 93.27% of their capacity after 100 cycles in SIBs. The study illustrates the self-segregation of elements from surface to bulk phase in the prepared HECMs. XPS spectroscopy suggests a proton exchange mechanism dominates in surface impurity generation, where exposed $Na_{0.79}Li_{0.13}Ni_{0.20}Mn_{0.67}O_2$ without doping (LNSM-0) reacts with air, exchanging Na^+ with H^+ on the surface, leading to impurity formation. In contrast, $Na_{0.79}Li_{0.13}Ni_{0.20}SS_{0.01}Mn_{0.66}O_2$, x = 0.01 (LNSM-0.01), with an enriched high-entropy region, prevents Na^+/H^+ exchange, inhibits impurity formation, and enhances air stability. Correspondingly, SEM images of exposed LNSM-0 display large clump impurities, while LNSM-0.01 exhibits uniform surface oxides formed during calcination. These oxides act as an artificial cathode-electrolyte interface (CEI) film, preventing impurity generation and reducing side reactions during cycling. (Figure 8E) The near-surface high-entropy area thereby improves air stability, reduces impurities, and stimulates anionic redox activity. DFT calculations further elucidate the synergistic effect based on entropy stability, reinforcing the layered oxide configuration for enhanced structural stability during cycling. This underscores not only technological advancements but also sustainable recycling possibilities for solid waste, accentuating the importance of materials recycling in the preparation of high-entropy electrode materials.

6. Summary and Outlook

The rational high-entropy design has addressed the electrochemical performance limitations of layered transition metal oxide cathodes and provided an effective solution for advancing sodium-ion battery performance. But it has been admitted that high-entropy layered oxides are still a nascent concept, and their complexity grows with the incorporation of various transition metals, posing challenges in terms of synthesis, characterization, and understanding of their intricate electrochemical behaviors. We lack a systematic theory that can explain the exact mechanism of HEOs, which can be used to guide the HEO design to improve electrochemical performance further. In this section, we will present both opportunities and challenges in developing high-performance HEOs for sustainable SIBs below.

1) **Clarifying mechanisms with advanced characterization techniques in Layered HEOs**. The analysis of layered high-entropy oxides presents formidable challenges due to their performance being a result of synergistic interactions among multiple components. Many of these elements, closely positioned in the chemical periodic table, share similarities in atomic masses, radii, and chemical properties. Current structural characterization of high-entropy materials relies on techniques such as XRD and Neutron Powder Diffraction (NPD) for phase composition determination. For elemental distribution, scanning electron microscopy coupled with energy-dispersive X-ray Spectroscopy and Scanning Transmission Electron Microscopy is employed. Probing the electronic structure and short-range geometries of metals in high-entropy materials is accomplished through X-ray absorption spectroscopy. Despite these techniques, conventional material characterization methods sometimes struggle to unravel the intricate structure and electrochemical reaction mechanisms of these materials precisely. Therefore, the utilization of advanced tools and methodologies like X-ray Pair

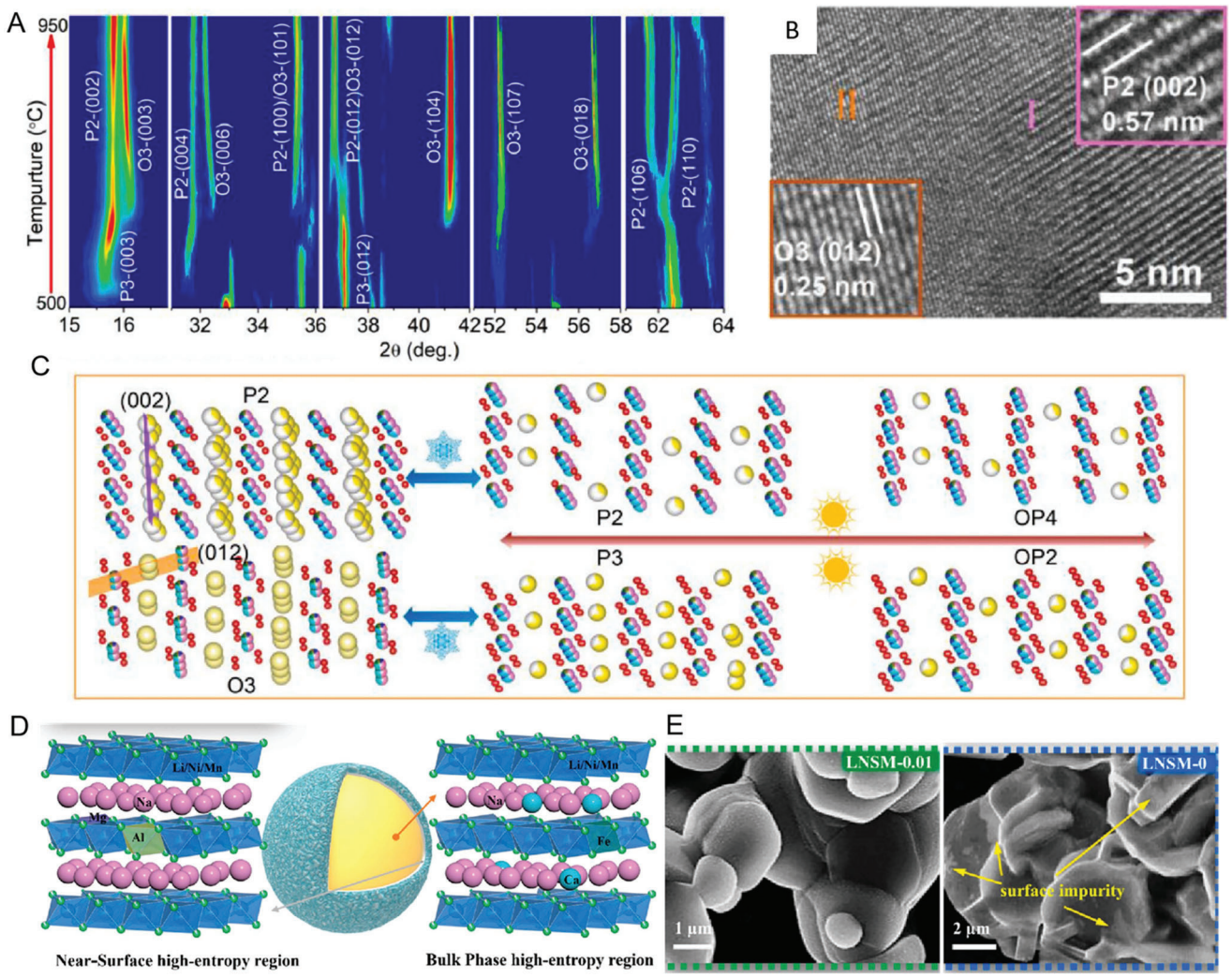

Figure 8. A) Disclosure of the P2/O3 biphasic structure generation by in situ XRD during the sintering process. B) HRTEM image of the biphasic HEO and C) structure evolution of the P2/O3 HEO upon charging/discharging. Reproduced with permission.[83] Copyright 2023, Elsevier. D) Schematic illustration of gradient HEO structure and E) the corresponding surface morphology of fresh and exposed LNSM-0.01and LNSM-0 sample. Reproduced with permission.[88] Copyright 2023, Elsevier.

Distribution Function (XPDF) becomes imperative for a comprehensive understanding of the complex relationship between material structure and electrochemical behavior, particularly during in situ/ex situ electrochemical processes.

2) **Achieving rational designed HEOs via machine learning and high-throughput screening**. The compositional design offers potential for tailoring high-entropy oxides' properties, but identifying functional units, understanding the role of individual elements, and dealing with the cocktail effect poses a significant challenge. Current studies are in an early stage, and the random nature of "tailoring" makes rational design challenging. Computational approaches, especially machine learning techniques, may aid in designing high-entropy materials with desired properties efficiently. Some ongoing challenges need to be addressed to foster machine learning-driven research on HEOs, including tackling the scarcity of diverse datasets, enhancing model interpretability, and developing convincing computational models based on the pool of comprehensive data from collaborative efforts. The complexity of high entropy materials, spanning multiple length scales, also calls for future research to explore multiscale modelling approaches, deepening insights into the intricate relationship between structure and properties.

3) **Synergizing phase engineering with HE designs to improve performance**. Both P2-and O3-type sodium layered oxides have their limitations for practical SIBs. The P2-type layer oxides possess faster diffusion kinetics and better surface and structure stability but lower specific capacity compared to O3 phase. By contrast, the O3-type oxides display higher energy density and ICE, but inferior cycle life and more severe structural degradation during cycling. A rational high-entropy design can overcome the limitations of both types of materials to some extent; however, it is still challenging to eliminate the drawbacks of each electrode material. Continued

exploration is imperative to comprehend the impact of configurational entropy on the structure of different layer HEOs. Accordingly, the integration of entropy control with phase engineering holds promise for capitalizing on the distinctive merits of two crystal phases, potentially leading to the realization of SIBs with superior energy density, high power capabilities, and extended cycle life.

4) **Considering commercial prospects and environmental impacts in the development of HEOs**. High entropy layered oxide materials with strong structural stability enable high-capacity retention and long cycle life. Future research endeavors should prioritize augmenting energy density and ensuring consistent sodium storage performance across a broader voltage range. The enhancement of initial Coulombic efficiency stands out as a critical objective for optimizing the overall electrochemical performance of cathode materials in full-cell applications. Additionally, there is an imperative to design cost-effective cathode materials, exemplified by systems such as Cu-Fe-Mn-based high entropy layered cathodes, leveraging the abundance of these elements. Furthermore, the intricate challenge of recyclability arises with the introduction of multiple elements in electrode materials. This presents novel obstacles in the recovery process and necessitates the development of innovative strategies for material characterization and recycling. It is worth mentioning that the investigation into layered cathode materials with superior thermal and air stability for SIBs is crucial. The careful selection of suitable elements for layered HEO cathode materials not only unlocks their inherent potential but also ensures their applicability across diverse practical scenarios. Addressing these multifaceted complexities will be pivotal in advancing the practical applications of high entropy layered oxide in the landscape of energy storage technologies.

In conclusion, this review provides a comprehensive overview of the intricate formation mechanisms of high-entropy materials, offering a detailed exploration of influential elements and the dynamic evolution of crystal and electronic structures during sodium (de)intercalation. The comprehensive analysis extends to the current research landscape, prospects, and the challenges encountered within the realm of high-entropy layered cathode materials for SIBs. This review emphasizes the tremendous potential of layered HEO cathode materials, which is expected to be a valuable reference for researchers immersed in the study of high-entropy materials and layer oxide cathode. Despite being in the early stages of the investigation, these materials show considerable promise, positioning them as key players in propelling the widespread adoption of cost-effective SIBs in energy storage systems in the foreseeable future.

Acknowledgements

H.G., J.L., and F.Z. contributed equally to this work. H.G. and Y.W. acknowledge the support from Open Project of State Key Laboratory of Advanced Special Steel, the Shanghai Key Laboratory of Advanced Ferrometallurgy, Shanghai University (SKLASS 2021-04), the Science and Technology Commission of Shanghai Municipality (22010500400) and "Shanghai Pujing Program" (23PJ1402800), "Joint International Laboratory on Environmental and Energy Frontier Materials" and "Innovation Research Team of High-Level Local Universities in Shanghai" at Shanghai University.

Open access publishing facilitated by University of Technology Sydney, as part of the Wiley - University of Technology Sydney agreement via the Council of Australian University Librarians.

Conflict of Interest

The authors declare no conflict of interest.

Keywords

formation mechanisms, high entropy effects, high-entropy materials, layered oxide cathode, sodium-ion batteries

Received: December 28, 2023
Revised: February 1, 2024
Published online: March 10, 2024

[1] Z. Zhu, T. Jiang, M. Ali, Y. Meng, Y. Jin, Y. Cui, W. Chen, *Chem. Rev.* **2022**, *122*, 16610.
[2] K. Kubota, M. Dahbi, T. Hosaka, S. Kumakura, S. Komaba, *Chem. Rec.* **2018**, *18*, 459.
[3] J. Chen, G. Zhang, J. Xiao, J. Li, Y. Xiao, D. Zhang, H. Gao, X. Guo, G. Wang, H. Liu, *Adv. Funct. Mater.* **2024**, *34*, 2307959.
[4] C. Vaalma, D. Buchholz, M. Weil, S. Passerini, *Nat. Rev. Mater.* **2018**, *3*, 18013.
[5] X. Guo, H. Gao, S. Wang, G. Yang, X. Zhang, J. Zhang, H. Liu, G. Wang, *Nano Lett.* **2022**, *22*, 1225.
[6] J. Li, L. Gao, F. Pan, C. Gong, L. Sun, H. Gao, J. Zhang, Y. Zhao, G. Wang, H. Liu, *Nano-Micro Lett.* **2024**, *16*, 12.
[7] J. Xiao, Y. Xiao, J. Li, C. Gong, X. Nie, H. Gao, B. Sun, H. Liu, G. Wang, *SmartMat* **2023**, *4*, e1211.
[8] Z. Li, T. Jiang, M. Ali, C. Wu, W. Chen, *Energy Storage Mater.* **2022**, *50*, 105.
[9] Y. Guo, C. Zhang, S. Xin, J. Shi, W. Wang, M. Fan, Y. Chang, W. He, E. Wang, Y. Zou, X. Yang, F. Meng, Y. Zhang, Z. Lei, Y. Yin, Y. Guo, *Angew. Chem., Int. Ed.* **2022**, *61*, e202116865.
[10] J. W. Sturman, E. A. Baranova, Y. Abu-Lebdeh, *Front. Energy Res.* **2022**, *10*, 862551.
[11] G. N. Kotsonis, S. S. I. Almishal, F. Marques dos Santos Vieira, V. H. Crespi, I. Dabo, C. M. Rost, J.-P. Maria, *J. Am. Ceram. Soc.* **2023**, *106*, 5587.
[12] J.-W. Yeh, *JOM* **2013**, *65*, 1759.
[13] E. J. Pickering, N. G. Jones, *Int. Mater. Rev.* **2016**, *61*, 183.
[14] E. P. George, D. Raabe, R. O. Ritchie, *Nat. Rev. Mater.* **2019**, *4*, 515.
[15] Y. F. Ye, Q. Wang, J. Lu, C. T. Liu, Y. Yang, *Mater. Today* **2016**, *19*, 349.
[16] X. Meng, X. Zhang, H. Sheng, M. Fan, T. Lin, D. Xiao, J. Tian, R. Wen, W. Liu, J. Shi, L. Wan, Y. Guo, *Angew. Chem., Int. Ed.* **2023**, *62*, e202302170.
[17] D. B. Miracle, O. N. Senkov, *Acta Mater.* **2017**, *122*, 448.
[18] K. Li, W. Chen, *Mater. Today Energy* **2021**, *20*, 100638.
[19] G. Zhang, G. Wan, (University of Science and Technology of China), CN114927663 A **2022**.
[20] H. Chen, F. Fu, X. Fu, (Huaqiao University), CN114927681 A **2022**.
[21] X. Gao, X. Zhang, X. Liu, Y. Tian, Q. Cai, M. Jia, X. Yan, *Small Methods* **2023**, *7*, 2300152.
[22] X. Zou, Y.-R. Zhang, Z.-P. Huang, K. Yue, Z.-H. Guo, *Chem. Commun.* **2023**, *59*, 13535.
[23] H. Sheng, X. Meng, D. Xiao, M. Fan, W. Chen, J. Wan, J. Tang, Y. Zou, F. Wang, R. Wen, J. Shi, Y. Guo, *Adv. Mater.* **2022**, *34*, 2108947.
[24] C. M. Rost, E. Sachet, T. Borman, A. Moballegh, E. C. Dickey, D. Hou, J. L. Jones, S. Curtarolo, J.-P. Maria, *Nat. Commun.* **2015**, *6*, 8485.

[25] C. Zhao, F. Ding, Y. Lu, L. Chen, Y.-S. Hu, *Angew. Chem., Int. Ed.* **2020**, *59*, 264.
[26] Z. Lun, B. Ouyang, D.-H. Kwon, Y. Ha, E. E. Foley, T.-Y. Huang, Z. Cai, H. Kim, M. Balasubramanian, Y. Sun, J. Huang, Y. Tian, H. Kim, B. D. McCloskey, W. Yang, R. J. Clément, H. Ji, G. Ceder, *Nat. Mater.* **2021**, *20*, 214.
[27] Y. Zeng, B. Ouyang, J. Liu, Y.-W. Byeon, Z. Cai, L. J. Miara, Y. Wang, G. Ceder, *Science* **2022**, *378*, 1320.
[28] R. Zhang, C. Wang, P. Zou, R. Lin, L. Ma, L. Yin, T. Li, W. Xu, H. Jia, Q. Li, S. Sainio, K. Kisslinger, S. E. Trask, S. N. Ehrlich, Y. Yang, A. M. Kiss, M. Ge, B. J. Polzin, S. J. Lee, W. Xu, Y. Ren, H. L. Xin, *Nature* **2022**, *610*, 67.
[29] P.-F. Wang, Y. You, Y.-X. Yin, Y.-G. Guo, *Adv. Energy Mater.* **2018**, *8*, 1701912.
[30] J. Xiao, X. Li, K. Tang, D. Wang, M. Long, H. Gao, W. Chen, C. Liu, H. Liu, G. Wang, *Mater. Chem. Front.* **2021**, *5*, 3735.
[31] C. Oses, C. Toher, S. Curtarolo, *Nat. Rev. Mater.* **2020**, *5*, 295.
[32] B. S. Murty, J. W. Yeh, S. Ranganathan, in *High-Entropy Alloys*, Butterworth-Heinemann, London **2014**.
[33] R. Z. Zhang, M. J. Reece, *J. Mater. Chem. A* **2019**, *7*, 22148.
[34] D. R. Gaskell, D. E. Laughlin, in *Introduction to the Thermodynamics of Materials*, CRC Press, Boca Raton, Florida, USA **2017**.
[35] P. H. Mayrhofer, A. Kirnbauer, P. Ertelthaler, C. M. Koller, *Scr. Mater.* **2018**, *149*, 93.
[36] A. Sarkar, B. Breitung, H. Hahn, *Scr. Mater.* **2020**, *187*, 43.
[37] A. Sarkar, R. Djenadic, N. J. Usharani, K. P. Sanghvi, V. S. K. Chakravadhanula, A. S. Gandhi, H. Hahn, S. S. Bhattacharya, *J. Eur. Ceram. Soc.* **2017**, *37*, 747.
[38] A. Sarkar, R. Djenadic, D. Wang, C. Hein, R. Kautenburger, O. Clemens, H. Hahn, *J. Eur. Ceram. Soc.* **2018**, *38*, 2318.
[39] M. Widom, *J. Mater. Res.* **2018**, *33*, 2881.
[40] Y. Ma, Y. Ma, Q. Wang, S. Schweidler, M. Botros, T. Fu, H. Hahn, T. Brezesinski, B. Breitung, *Energy Environ. Sci.* **2021**, *14*, 2883.
[41] Y. Yao, Q. Dong, A. Brozena, J. Luo, J. Miao, M. Chi, C. Wang, I. Kevrekidis, Z. Ren, J. Greeley, G. Wang, A.-A. Sky, L. Hu, *Science* **2022**, *376*, eabn3103.
[42] Y. Chen, H. Fu, Y. Huang, L. Huang, X. Zheng, Y. Dai, Y. Huang, W. Luo, *ACS Mater. Lett.* **2021**, *3*, 160.
[43] S. H. Albedwawi, A. AlJaberi, G. N. Haidemenopoulos, K. Polychronopoulou, *Mater. Des.* **2021**, *202*, 109534.
[44] Y. Sun, S. Dai, *Sci. Adv.* **2021**, *7*, eabg1600.
[45] L. Su, X. Chen, L. Xu, T. Eldred, J. Smith, C. DellaRova, H. Wang, W. Gao, *ACS Nano* **2022**, *16*, 21397.
[46] Y. Dong, K. Ren, Y. Lu, Q. Wang, J. Liu, Y. Wang, *J. Eur. Ceram. Soc.* **2019**, *39*, 2574.
[47] Z. Zhao, H. Chen, H. Xiang, F.-Z. Dai, X. Wang, W. Xu, K. Sun, Z. Peng, Y. Zhou, *J. Mater. Sci. Technol.* **2020**, *47*, 45.
[48] D. Bérardan, S. Franger, A. K. Meena, N. Dragoe, *J. Mater. Chem. A* **2016**, *4*, 9536.
[49] D. Wang, S. Jiang, C. Duan, J. Mao, Y. Dong, K. Dong, Z. Wang, S. Luo, Y. Liu, X. Qi, *J. Alloys Compd.* **2020**, *844*, 156158.
[50] T. Jin, X. Sang, R. R. Unocic, R. T. Kinch, X. Liu, J. Hu, H. Liu, S. Dai, *Adv. Mater.* **2018**, *30*, 1707512.
[51] T. Wang, H. Chen, Z. Yang, J. Liang, S. Dai, *J. Am. Chem. Soc.* **2020**, *142*, 4550.
[52] A. Sarkar, Q. Wang, A. Schiele, M. R. Chellali, S. S. Bhattacharya, D. Wang, T. Brezesinski, H. Hahn, L. Velasco, B. Breitung, *Adv. Mater.* **2019**, *31*, 1806236.
[53] J.-L. Yue, Y.-N. Zhou, X. Yu, S.-M. Bak, X.-Q. Yang, Z.-W. Fu, *J. Mater. Chem. A* **2015**, *3*, 23261.
[54] J.-L. Yue, W.-W. Yin, M.-H. Cao, S. Zulipiya, Y.-N. Zhou, Z.-W. Fu, *Chem. Commun.* **2015**, *51*, 15712.
[55] K. Tian, H. He, X. Li, D. Wang, Z. Wang, R. Zheng, H. Sun, Y. Liu, Q. Wang, *J. Mater. Chem. A* **2022**, *10*, 14943.
[56] M. Sathiya, Q. Jacquet, M.-L. Doublet, O. M. Karakulina, J. Hadermann, J.-M. Tarascon, *Adv. Energy Mater.* **2018**, *8*, 1702599.
[57] J. B. Goodenough, *Mol. Cryst. Liq. Cryst.* **2006**, *311*, 1
[58] K. Walczak, A. Plewa, C. Ghica, W. Zając, A. Trenczek-Zając, M. Zając, J. Toboła, J. Molenda, *Energy Storage Mater.* **2022**, *47*, 500.
[59] B. Ouyang, J. Wang, T. He, C. J. Bartel, H. Huo, Y. Wang, V. Lacivita, H. Kim, G. Ceder, *Nat. Commun.* **2021**, *12*, 5752.
[60] N. J. Szymanski, Y. Zeng, H. Huo, C. J. Bartel, H. Kim, G. Ceder, *Mater. Horiz.* **2021**, *8*, 2169.
[61] J. Sturman, C.-H. Yim, E. A. Baranova, Y. Abu-Lebdeh, *J. Electrochem. Soc.* **2021**, *168*, 050541.
[62] Q. Wang, L. Velasco, B. Breitung, V. Presser, *Adv. Energy Mater.* **2021**, *11*, 2102355.
[63] V. Sulzer, P. Mohtat, A. Aitio, S. Lee, Y. T. Yeh, F. Steinbacher, M. U. Khan, J. W. Lee, J. B. Siegel, A. G. Stefanopoulou, D. A. Howey, *Joule* **2021**, *5*, 1934.
[64] K. A. Severson, P. M. Attia, N. Jin, N. Perkins, B. Jiang, Z. Yang, M. H. Chen, M. Aykol, P. K. Herring, D. Fraggedakis, M. Z. Bazant, S. J. Harris, W. C. Chueh, R. D. Braatz, *Nat. Energy* **2019**, *4*, 383.
[65] C. Zhao, Y. Lu, L. Chen, Y.-S. Hu, *Nano Res.* **2019**, *12*, 2018.
[66] H. Pan, Y.-S. Hu, L. Chen, *Energy Environ. Sci.* **2013**, *6*, 2338.
[67] C. Delmas, C. Fouassier, P. Hagenmuller, *Physica B+C* **1980**, *99*, 81.
[68] T. Cai, M. Cai, J. Mu, S. Zhao, H. Bi, W. Zhao, W. Dong, F. Huang, *Nano-Micro Lett.* **2024**, *16*, 10.
[69] J. Zhang, W. Wang, W. Wang, S. Wang, B. Li, *ACS Appl. Mater. Interfaces* **2019**, *11*, 22051.
[70] J.-M. Kim, X. Zhang, J.-G. Zhang, A. Manthiram, Y. S. Meng, W. Xu, *Mater. Today* **2021**, *46*, 155.
[71] B. Peng, Y. Chen, F. Wang, Z. Sun, L. Zhao, X. Zhang, W. Wang, G. Zhang, *Adv. Mater.* **2022**, *34*, 2307959.
[72] X. Li, D. Wu, Y.-N. Zhou, L. Liu, X.-Q. Yang, G. Ceder, *Electrochem. Commun.* **2014**, *49*, 51.
[73] X. Rong, E. Hu, Y. Lu, F. Meng, C. Zhao, X. Wang, Q. Zhang, X. Yu, L. Gu, Y.-S. Hu, H. Li, X. Huang, X.-Q. Yang, C. Delmas, L. Chen, *Joule* **2019**, *3*, 503.
[74] D. Yuan, X. Liang, L. Wu, Y. Cao, X. Ai, J. Feng, H. Yang, *Adv. Mater.* **2014**, *26*, 6301.
[75] C.-C. Lin, H.-Y. Liu, J.-W. Kang, C.-C. Yang, C.-H. Li, H.-Y. T. Chen, S.-C. Huang, C.-S. Ni, Y.-C. Chuang, B.-H. Chen, C.-K. Chang, H.-Y. Chen, *Energy Storage Mater.* **2022**, *51*, 159.
[76] F. Ding, C. Zhao, D. Xiao, X. Rong, H. Wang, Y. Li, Y. Yang, Y. Lu, Y.-S. Hu, *J. Am. Chem. Soc.* **2022**, *144*, 8286.
[77] Z. Hu, M. Weng, Z. Chen, W. Tan, S. Li, F. Pan, *Nano Energy* **2021**, *83*, 105834.
[78] L. Yao, P. Zou, C. Wang, J. Jiang, L. Ma, S. Tan, K. A. Beyer, F. Xu, E. Hu, H. L. Xin, *Adv. Energy Mater.* **2022**, *12*, 2201989.
[79] D. A. Anang, J.-H. Park, D. S. Bhange, M. K. Cho, W. Y. Yoon, K. Y. Chung, K.-W. Nam, *Ceram. Int.* **2019**, *45*, 23164.
[80] L. Yang, C. Chen, S. Xiong, C. Zheng, P. Liu, Y. Ma, W. Xu, Y. Tang, S. P. Ong, H. Chen, *JACS Au* **2021**, *1*, 98.
[81] S. Yan, S. Luo, L. Yang, J. Feng, P. Li, Q. Wang, Y. Zhang, X. Liu, *J. Adv. Ceram.* **2022**, *11*, 158.
[82] H. Wang, X. Gao, S. Zhang, Y. Mei, L. Ni, J. Gao, H. Liu, N. Hong, B. Zhang, F. Zhu, W. Deng, G. Zou, H. Hou, X. Cao, H. Chen, X. Ji, *ACS Nano* **2023**, *17*, 12530.
[83] P. Zhou, Z. Che, J. Liu, J. Zhou, X. Wu, J. Weng, J. Zhao, H. Cao, J. Zhou, F. Cheng, *Energy Storage Mater.* **2023**, *57*, 618.
[84] F. Fu, X. Liu, X. Fu, H. Chen, L. Huang, J. Fan, J. Le, Q. Wang, W. Yang, Y. Ren, K. Amine, S.-G. Sun, G.-L. Xu, *Nat. Commun.* **2022**, *13*, 2826.
[85] F. Ding, H. Wang, Q. Zhang, L. Zheng, H. Guo, P. Yu, N. Zhang, Q. Guo, F. Xie, R. Dang, X. Rong, Y. Lu, R. Xiao, L. Chen, Y. Hu, *J. Am. Chem. Soc.* **2023**, *145*, 13592.

[86] J. Wang, Y. Cui, Q. Wang, K. Wang, X. Huang, D. Stenzel, A. Sarkar, R. Azmi, T. Bergfeldt, S. S. Bhattacharya, R. Kruk, H. Hahn, S. Schweidler, T. Brezesinski, B. Breitung, *Sci. Rep.* **2020**, *10*, 18430.
[87] Q. Zheng, Z. Ren, Y. Zhang, T. Qin, J. Qi, H. Jia, L. Jiang, L. Li, X. Liu, L. Chen, *ACS Appl. Mater. Interfaces* **2023**, *15*, 4643.
[88] J. Feng, Y. Liu, D. Fang, J. Li, *Nano Energy* **2023**, *118*, 109030.
[89] J. Mu, T. Cai, W. Dong, C. Zhou, Z. Han, F. Huang, *Chem. Eng. J.* **2023**, *471*, 144403.
[90] Y. Dang, Z. Xu, H. Yang, K. Tian, Z. Wang, R. Zheng, H. Sun, Y. Liu, D. Wang, *Appl. Surf. Sci.* **2023**, *636*, 157856.
[91] P. Zhou, Z. Che, J. Liu, J. Zhou, X. Wu, J. Weng, J. Zhao, H. Cao, J. Zhou, F. Cheng, *Energy Storage Mater.* **2023**, *57*, 618.
[92] H. Deng, L. Liu, Z. Shi, *Mater. Lett.* **2023**, *340*, 134113.
[93] M. Nowak, K. Walczak, A. Milewska, J. Płotek, A. Budziak, J. Molenda, *J. Alloys Compd.* **2023**, *968*, 172316.
[94] T. Cai, M. Cai, J. Mu, S. Zhao, H. Bi, W. Zhao, W. Dong, F. Huang, *Nano-Micro Lett.* **2023**, *16*, 10.
[95] S. Ma, P. Zou, H. L. Xin, *Mater. Today Energy* **2023**, *38*, 101446.
[96] X.-Y. Du, Y. Meng, H. Yuan, D. Xiao, *Energy Storage Mater.* **2023**, *56*, 132.
[97] J. Wang, S. L. Dreyer, K. Wang, Z. Ding, T. Diemant, G. Karkera, Y. Ma, A. Sarkar, B. Zhou, M. V. Gorbunov, A. Omar, D. Mikhailova, V. Presser, M. Fichtner, H. Hahn, T. Brezesinski, B. Breitung, Q. Wang, *Mater. Futures* **2022**, *1*, 035104.
[98] H. Guo, M. Avdeev, K. Sun, X. Ma, H. Wang, Y. Hu, D. Chen, *Chem. Eng. J.* **2021**, *412*, 128704.
[99] Z.-Y. Li, R. Gao, L. Sun, Z. Hu, X. Liu, *Electrochim. Acta* **2017**, *223*, 92.

Hong Gao is presently serving as an Associate Professor at Shanghai University. She completed her Ph.D. in Material Science at the University of Wollongong, Australia, in 2018. Following her doctoral studies, she assumed the role of faculty postdoctoral fellow at Shanghai University before transitioning to the University of Technology Sydney as a Research Associate. Her research pursuits center on the synthesis and applications of advanced functional materials tailored for energy storage and conversion applications.

Guoxiu Wang is the director of the Centre for Clean Energy Technology and a distinguished professor at University of Technology Sydney (UTS), Australia. His research interests include lithium-ion batteries, lithium–air batteries, sodium-ion batteries, lithium–sulfur batteries, supercapacitors, hydrogen storage materials, fuel-cells, 2D materials such as graphene and MXene, and electrocatalysis for hydrogen production. Professor Wang has published more than 650 refereed journal papers with an h-index of 144. His publications have attracted over 67 000 citations. He has been recognized as a highly cited researcher in both Materials Science and Chemistry by Clarivate Analytics.

Hao Liu is a Full Professor and ARC Future Fellow at University of Technology Sydney (UTS). He obtained his PhD degree from the University of Wollongong in 2011. He worked as a research associate at the University of Queensland and moved to the University of Technology Sydney as a Chancellor's postdoctoral research fellow. He is interested in the synthesis of nanostructured materials and their applications in the fields of lithium-ion batteries, sodium-ion batteries, lithium–sulfur batteries, lithium–oxygen batteries, supercapacitors, and electrocatalysts.